SPECIAL PROJECT

ON

THE EFFECTS OF WATER IMPINGING ON THERMALLY-CONTROLLED SURFACES UNDER SPACE CONDITIONS

NATIONAL AERONAUTICS AND SPACE ADMINISTRATION
MARSHALL SPACE FLIGHT CENTER
MULTIDISCIPLINARY RESEARCH GRANT
NGR-19-001-68

Report Prepared by

Dr. D. Maples
Mr. M. H. Spiller
Department of Mechanical and
Aerospace Engineering
College of Engineering
Louisiana State University
Baton Rouge, Louisiana 70803

SPECIAL PROJECT

ON

THE EFFECTS OF WATER IMPINGING ON THERMALLY-CONTROLLED SURFACES UNDER SPACE CONDITIONS

NATIONAL AERONAUTICS AND SPACE ADMINISTRATION
MARSHALL SPACE FLIGHT CENTER
MULTIDISCIPLINARY RESEARCH GRANT
NGR-19-001-68

Report Prepared by

Dr. D. Maples
Mr. M. H. Spiller
Department of Mechanical and
Aerospace Engineering
College of Engineering
Louisiana State University
Baton Rouge, Louisiana 70803

ACKNOWLEDGMENTS

The author wishes to extend his deep appreciation and thanks to the following individuals and organizations for their assistance during this research:

Dr. Dupree Maples, who served as major professor, for his guidance and assistance.

Mr. Marshall King for making available paint samples and supplying technical information pertaining to these samples.

Mr. Riddle Steddum for his encouragement and technical discussions throughout this study.

Dr. W. A. Wiebelt for his contributions of important data.

Mississippi Test Facility for use of their equipment and facilities during this research.

National Aeronautics and Space Administration for funding this investigation.

My father and sister for many helpful improvements in the manuscript and its typing.

TABLE OF CONTENTS

LIST OF FIGURES

ABSTRACT

The results of an investigation to experimentally determine the monochromatic reflectance changes caused from an impinging water spray on thermally-controlled paints are presented. After reaching thermal equilibrium with their space environment, the paint samples were struck with water ejected from a sharp-edge nozzle. An integrating sphere was constructed to measure the reflectance changes after exposure to the water jet.

Inconclusive results were obtained because the water droplets failed to freeze solidly before impingement. High speed motion pictures taken of the spray during impact showed the particles consisted of thin shells of ice with liquid centers. Visible surface damage occurred to one of the paints (Z93), although the integrating sphere was unable to measure a change in reflectance.

CHAPTER I

INTRODUCTION

One of America's proposed space goals is to orbit a workshop in 1972, using an SIVB booster as the basis for that spacecraft. Many technical questions must be answered before this objective can become a reality. Among the problems to be solved is the disposal of human and other wastes, such as, non-potable water generated in the operation of solar cells, that would develop during long stays in space.

A probable solution is the venting of waste into the space environment. While this answers the immediate problem, other difficulties could arise as a result of this action and should be investigated prior to reaching a final decision as to the method of disposal. For instance, there is a possibility that an ice cloud, orbiting with the workshop, would form from the vented fluids and decrease the efficiency of the Apollo telescope. Another problem that would arise is the effect vented fluids would have on thermally-controlled surfaces of the spacecraft when struck by ejected fluids, which is the objective of this research.

The development and selection of surface materials for exposure to a harsh space environment is a difficult and complex problem. These surface materials are required to survive long periods in a space environment while maintaining their desirable thermally-controlled properties. Along with the natural hazards of a space environment, such as extremely low pressures, micrometeorite bombardment, and variable extreme

temperatures, there are man-made hazards which these coatings must endure during the operation of a space vehicle.

The purpose of this study is to investigate experimentally the effects of water vented from a spacecraft and striking a thermally-controlled surface. The investigation arose from work performed by Mr. Riddle Steddum and Dr. Dupree Maples while studying velocities of fluid particles that had been vented into a space environment. They noticed the effects of the water spray on a piece of aluminum foil placed in the chamber during one of their experiments. It was decided that a few selected thermally-controlled paints and aluminum foil would be subjected to a water spray, and the change in surface properties would be recorded.

Mr. Marshall King of the NASA Marshall Space Flight Center prepared samples of three paints for this investigation. Two of the paint samples (Z93 and S13G) are presently being used on the proposed new space workshop; the third paint sample (92-007) is the back-up paint for the forementioned two. All of these paints have low solar absorptance which gives rise to highly reflective surfaces.

The amount of reflected energy is highly dependent upon the wavelength of the incoming solar energy. With this in mind, it was decided that the best method of describing the effects of the water jet impinging on these surfaces was to measure the change in monochromatic reflectance of the aluminum foil and paint samples. To accomplish this task, an integrating sphere reflectometer was constructed. The integrating sphere provides the capability to measure the directional monochromatic reflectance of the samples before and after exposure to the water jet. These readings are the means of evaluating the degree of degradation of the samples caused by their exposure to the water jet.

CHAPTER II

THEORY OF THE INTEGRATING SPHERE

View Factor Consideration

The basis of an integrating sphere is the view factor between any two points on the inner spherical wall is identical to any other two points within the sphere. Wiebelt [9]* defines configuration factor (view factor) as the fraction of energy directly incident on one surface, from another surface assumed to be emitting diffusely. The result of these identical view factors within the sphere is that the incoming energy is uniformly distributed over the entire spherical walls. The proof [10] of the identical view factors follows.

Let us examine a two-dimensional representation of a sphere having diffused walls. If two arbitrary small areas (dA_1, dA_2) are chosen inside the sphere, the view factor between these two areas will be obtained. The radiant energy leaving surface element dA_1 that is directly incident on dA_2 is

$$I_1 \cos\phi_1 \, dA_1 \, dw_{12} \qquad \text{(II-1)}$$

*Numbers in brackets indicate references in the bibliography.

where,

I_1 = Intensity of energy leaving dA_1

$\emptyset_1$ = Angle between R_{12} and the normal to dA_1

R_{12} = Straight line distance between dA_1 and dA_2

dw_{12} = Solid angle through which dA_1 views dA_2

Within a sphere the solid angle formed between two differential areas is the projected area viewed divided by the square of the straight line distance between the two differential areas, i.e.:

$$dw_{12} = \frac{\cos \emptyset_2 dA_2}{R_{12}^2} \qquad \text{(II-2)}$$

Substituting equation II-2 into II-1, equation II-3 is obtained

$$\frac{I_1 \cos \emptyset_1 \cos \emptyset_2 \, dA_1 \, dA_2}{R_{12}^2} \qquad \text{(II-3)}$$

Equation II-3 is the energy leaving surface one that is directly incident on surface two.

Using the definition of view factor, it is shown that the view factor from dA_1 to dA_2 is represented by

$$F_{dA_1 \rightarrow dA_2} = \frac{I_1 \cos \emptyset_1 \cos \emptyset_2 \, dA_1 \, dA_2}{R_{12}^2 \, I_1 \, \pi \, dA_1} \qquad \text{(II-4)}$$

$$F_{dA_1 \rightarrow dA_2} = \frac{\cos \emptyset_1 \cos \emptyset_2 \, dA_2}{\pi \, R_{12}^2} \qquad \text{(II-4a)}$$

where,

$F_{dA_1 \longrightarrow dA_2}$ = View factor between surfaces 1 and 2.

$I_1 \pi \, dA_1$ = Total energy leaving surface 1.

Since the normal to any surface area on a sphere passes through the center of the sphere, the angles ϕ_1 and ϕ_2 are equal, which reduces equation II-4a to

$$F_{dA_1 \longrightarrow dA_2} = \frac{\cos^2 \phi \, dA_2}{\pi \, R_{12}^2} \tag{II-5}$$

If a perpendicular is constructed at the midpoint of R_{12}, the perpendicular passes through the center of the sphere, forming two right triangles (see Figure II-1). Using trigonometric relations, the following is derived:

$$\cos \phi_1 = \frac{R_{12}}{2R} \tag{II-6}$$

$$\frac{\cos^2 \phi_1}{R_{12}^2} = \frac{1}{4R^2} \tag{II-6a}$$

Since $\phi_1 = \phi_2 = \phi$

$$\frac{\cos^2 \phi}{R_{12}^2} = \frac{1}{4R^2} \tag{II-7}$$

Substituting equation II-7 into II-5, equation II-8 is obtained.

$$F_{dA_1 \longrightarrow dA_2} = \frac{1}{4\pi R^2} \, dA_2 \tag{II-8}$$

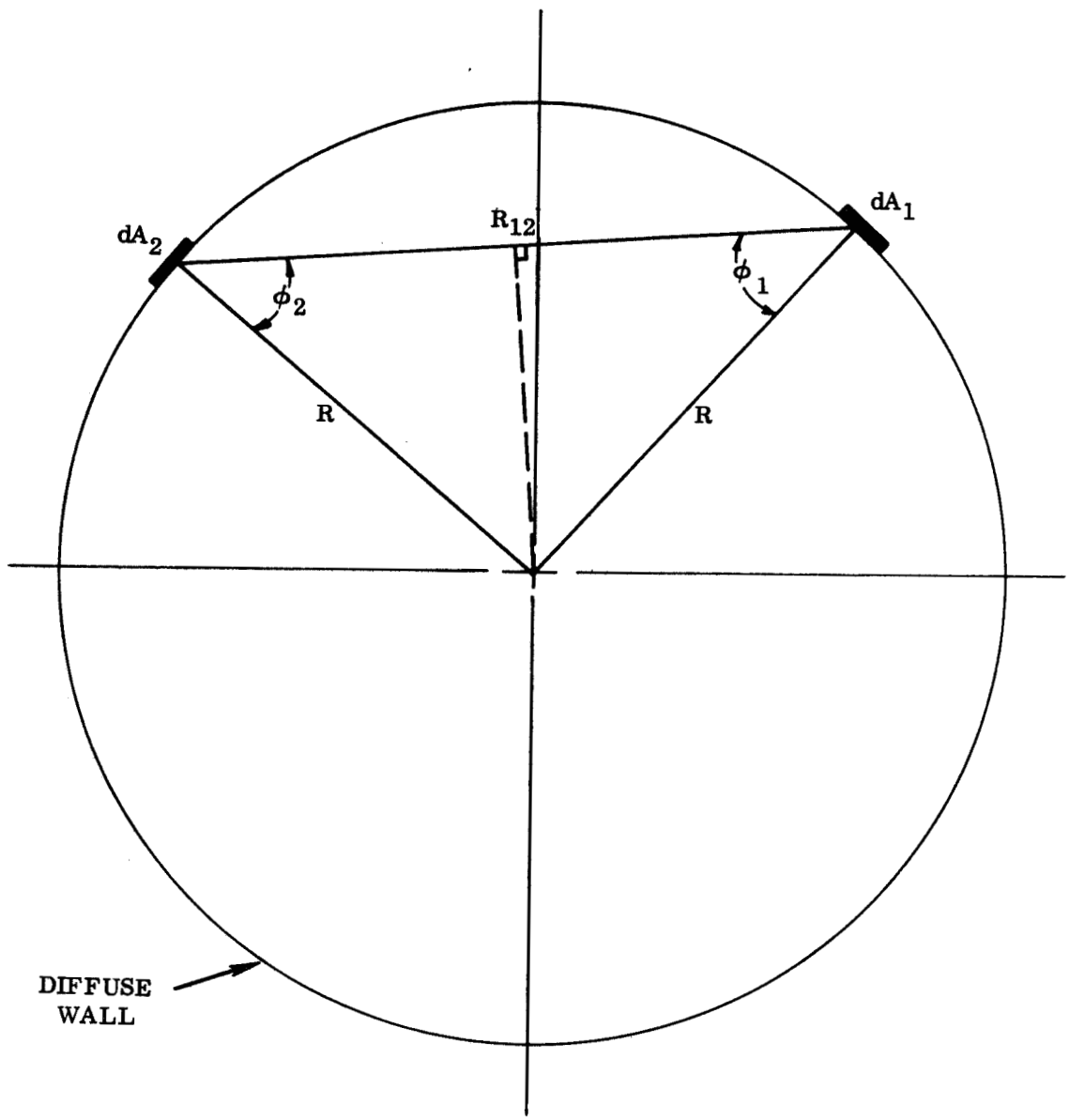

Figure II-1 Geometry of an
Integrating Sphere

Equation II-8 proves that the view factor between any two differential areas is independent of the position of the areas chosen. Since the areas chosen in this proof were arbitrary, it can be concluded that the view factor between any two points inside a spherical surface are identical to any other two points within that sphere.

Reflectance Measurement

To determine the directional hemispherical reflectance (Figure II-2) of a sample using an integrating sphere, two measurements are necessary.

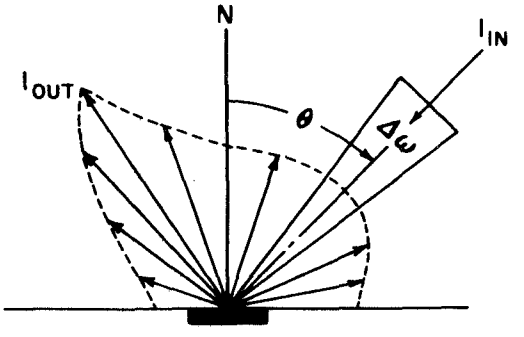

FIGURE II - 2 DIRECTIONAL HEMISPHERICAL REFLECTANCE

The first measurement is the signal response recorded from a detector when a monochromatic beam of energy is directly incident on the diffuse wall. A portion of the energy leaving the wall is directly incident on the detector while the remaining energy is reflected throughout the sphere. Due to multiple reflections within the sphere, the incoming beam is evenly distributed throughout the entire sphere. The second measurement is again the electrical response of a detector viewing the

inner surface of the sphere. The sample to be measured is placed in the path of the incoming beam. A portion of the beam's energy is absorbed by the sample while the remaining energy is reflected to the sphere's wall. Figure II-3 shows a two-dimensional view of a light beam incident on a sample. To obtain a measurement without the sample's interference, the sample was rotated out of the path of the incoming light. Special attention was given to the placement of the detectors to prevent the reflected light from the sample from becoming directly incident on the detectors. The ratio of the two signals is the total directional hemispherical reflectance of the surface under investigation.

Three basic assumptions are made when measuring reflectance with an integrating sphere. First, the spherical wall is completely diffuse; secondly, the loss of energy through the entrance is negligible; and, finally, the sample, sample holder, and detectors do not significantly affect interreflections. A further examination into the inherent errors involved using an integrating sphere will be discussed later in this chapter.

Under the basic assumptions, the signal detected when a beam is directly incident on the wall of the sphere is written as

$$S_1 = \int_{A_d} \int_{A_s} \frac{K\, I \cos \phi_1 \cos \phi_2}{R_{12}^2} \, dA_d \, dA_s \qquad \text{(II-9)}$$

where K is the sensitivity of the detector, I is the intensity of the source, A_d is the area of the detector, A_s is the area of the energy striking the sphere, and R_{12}, ϕ_2 are as defined previously.

Assuming the sensitivity of the detectors are not angular, the

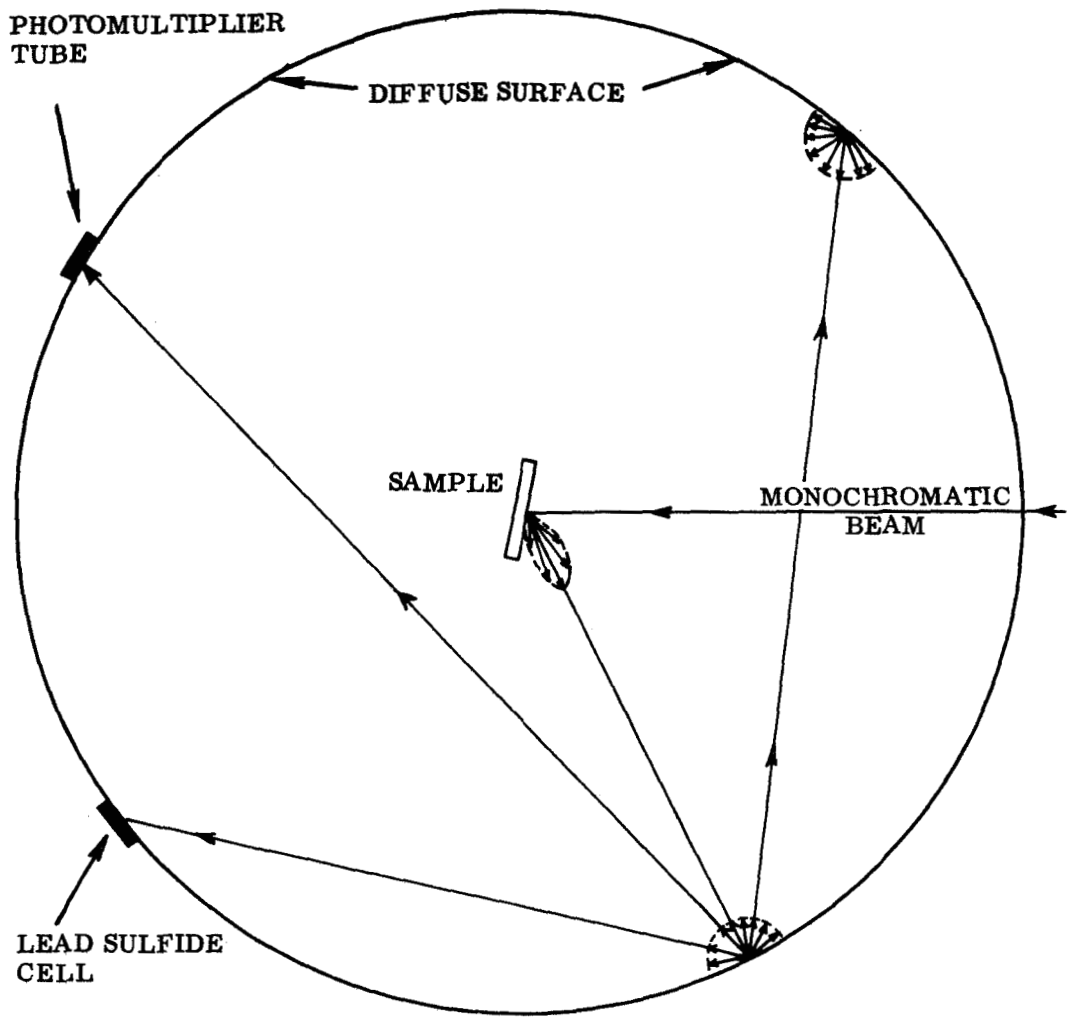

Figure II-3 Sample in Beam's Path for
Reflectance Measurement

wall is completely diffuse and substituting equation II-7 into II-9, it is found that

$$S_1 = \frac{K}{4R^2} \int_{A_d} \int_{A_s} I \, dA_d \, dA_s \qquad \text{(II-10)}$$

Under the assumption that the detector area does not affect significantly the interreflections, equation II-10 reduces to

$$S_1 = \frac{KA_d}{4R^2} \int_{A_s} I \, dA_s \qquad \text{(II-11)}$$

For the case of diffuse reflectors in an enclosure

$$I = \frac{J}{\pi} \qquad \text{(II-12)}$$

where J as defined by Wiebelt [9] is the total radiant power leaving the surface of a system per unit area of surface, thus equation II-12 becomes

$$S_1 = \frac{K A_d}{4 \pi R^2} \int_{A_s} J dA_s \qquad \text{(II-13)}$$

If we consider the radiant power associated with the incoming beam as E, the radiosity of the spherical wall related to this power can be written as

$$\int_{A_s} J dA_s = E + \rho E + \rho^2 E + \rho^3 E + \ldots \qquad \text{(II-14)}$$

where ρ is defined as the reflectance of the diffuse wall. The first

term, E, is the energy associated with the incoming beam. The second term is the energy leaving after the first reflection; the third term is the energy leaving after the second reflection. The process of inter-reflection is continuous. The amount of energy reflected each time is equal to the reflectance of the wall times the amount of energy reflected on the previous reflection. The right-hand side of equation II-14 can be represented as an infinite series whose sum is

$$E\left[\frac{1}{1-\rho}\right], \quad \rho < 1 \tag{II-15}$$

Hence, equation II-13 can be expressed as

$$S_1 = \frac{KA_dE}{4\pi R^2}\left(\frac{1}{1-\rho}\right) \tag{II-16}$$

A similar analysis can be made when the sample is rotated into the beam. An additional reflectance term (ρ_s) is present in the equation due to the reflectance of the sample. The radiosity of the wall with the sample in the beam's path is written as

$$\int_{A_s} JdA_s = \rho_s E + \rho_s\rho E + \rho_s\rho^2 E + \rho_s\rho^3 E + \ldots \tag{II-17}$$

As before equation II-17 can be reduced to,

$$\int_{A_s} JdA_s = \rho_s E\left[\frac{1}{1-\rho}\right], \quad \rho < 1 \tag{II-18}$$

Therefore the signal recorded when the sample is in the beam's path is

$$S_2 = \frac{KA_dE}{4\pi R^2} \rho_s \left(\frac{1}{1-\rho} \right) \qquad \text{(II-19)}$$

Taking the ratio of the two signals, the directional hemispherical reflectance is:

$$S_2 / S_1 = \frac{KA_dE}{4\pi R^2} \rho_s \left(\frac{1}{1-\rho} \right) \Big/ \frac{KA_dE}{4\pi R^2} \left(\frac{1}{1-\rho} \right) \qquad \text{(II-20)}$$

$$\rho_s = S_2 / S_1 \qquad \text{(II-21)}$$

This particular equation was used to evaluate all reflectance values during this investigation.

Errors Inherent in Integrating Spheres

The integrating sphere, although simple to construct, must be carefully planned prior to construction. Significant errors in reflectance values are obtained if care is not taken in locating the detectors, the sample, and the entrance port. Early investigators placed their samples as part of the spherical wall. This procedure was followed to insure that view factors remain constant over the entire sphere and also to prevent shadowing as a result of an obstruction within the sphere. Safwatt [6] investigated the effects of a centrally located sample and determined that if the proper ratio of sample area to spherical area was maintained, the errors in measured reflectance

were small.

Newnam [5] presented a thorough discussion of the sources of error inherent to an integrating sphere reflectometer. To properly design and evaluate its performance, the following sources of error must be evaluated:

1. Direct irradiation of the detectors without reflection from the sphere wall
2. Nonuniformity of the sphere wall coating
3. Entrance port losses
4. Nondiffuseness of sphere wall
5. Shadowing by sample holder
6. Interreflection with sample
7. Nonlinearity of detection system
8. Flourescence of the sample
9. Stray radiation
10. Polarization by monochromator optics

Newnam evaluated the magnitude of these errors for an integrating sphere design by Edwards [2]. The total error in reflectance was discovered to be $\pm$ (1.5% + .005). A discussion of Newnam's sources of error as applied to the integrating sphere used in this research will be discussed later.

CHAPTER III

EXPERIMENTAL APPARATUS AND INSTRUMENTATION

Space Simulation Chamber

The paint samples were subjected to the water spray in a Murphy and Miller Vacuum Chamber located at the National Aeronautics and Space Administration's Mississippi Test Facility. The vacuum chamber and its controls are shown in Figure III-1. The chamber, which measures 47 inches in diameter and 60 inches long, was evacuated by a Stokes mechanical roughing pump and an oil diffusion pump. This particular evacuation system was able to produce and maintain a pressure during testing of approximately 1.0×10^{-5} torr. The chamber pressure was measured with a Logatorr unit consisting of a thermocouple gauge and an ionization gauge.

The chamber is equipped with four viewing ports that enable the researcher to view and to take high speed motion pictures of the bombardment of paint samples. In addition to these viewing ports, a 24 inch diameter aluminum flange (Figure III-2) was bolted to the chamber to allow instrumentation and power feedthroughs. A Consolidated Vacuum rotary-mechanical feedthrough is mounted on the flange to allow mechanical motion in the chamber during testing. A glass port was installed in the center of the flange to provide an additional side viewing port.

Because the vacuum chamber was designed originally for high altitude simulation and not to simulate space conditions, it was

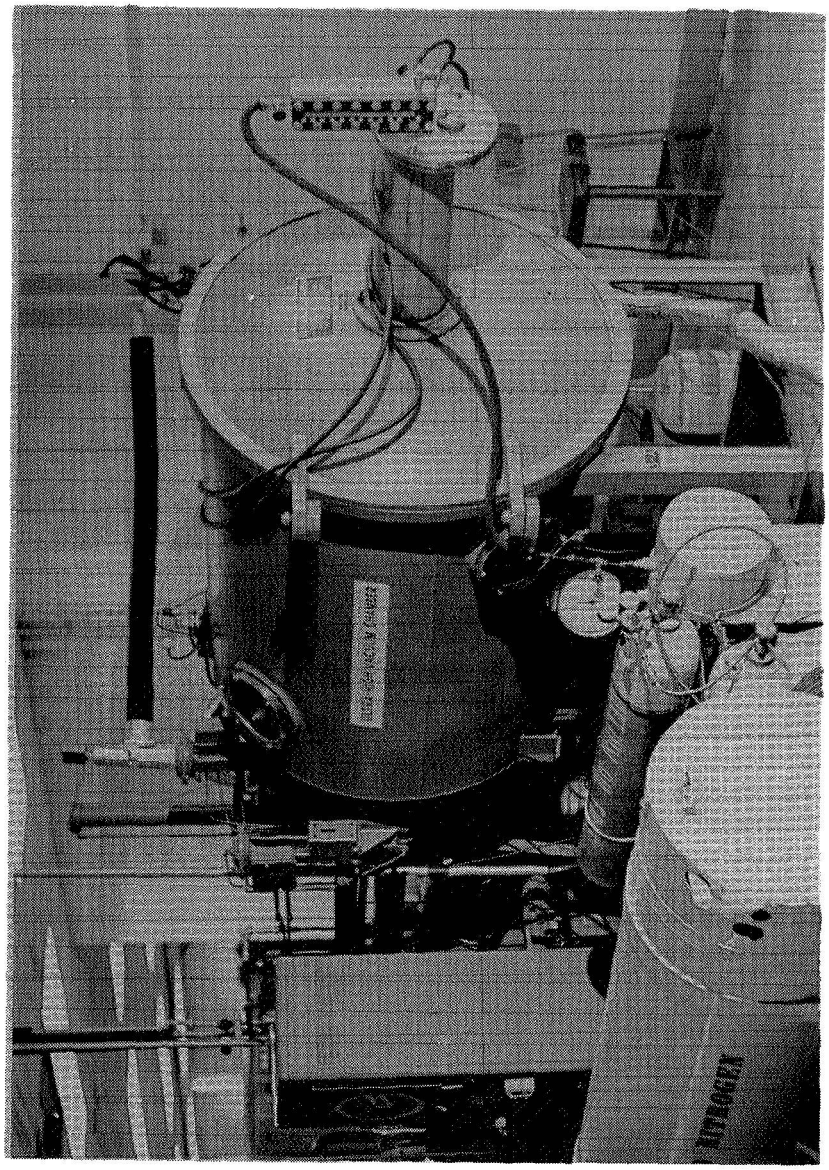

Figure III-1 Overall View of Simulation Chamber

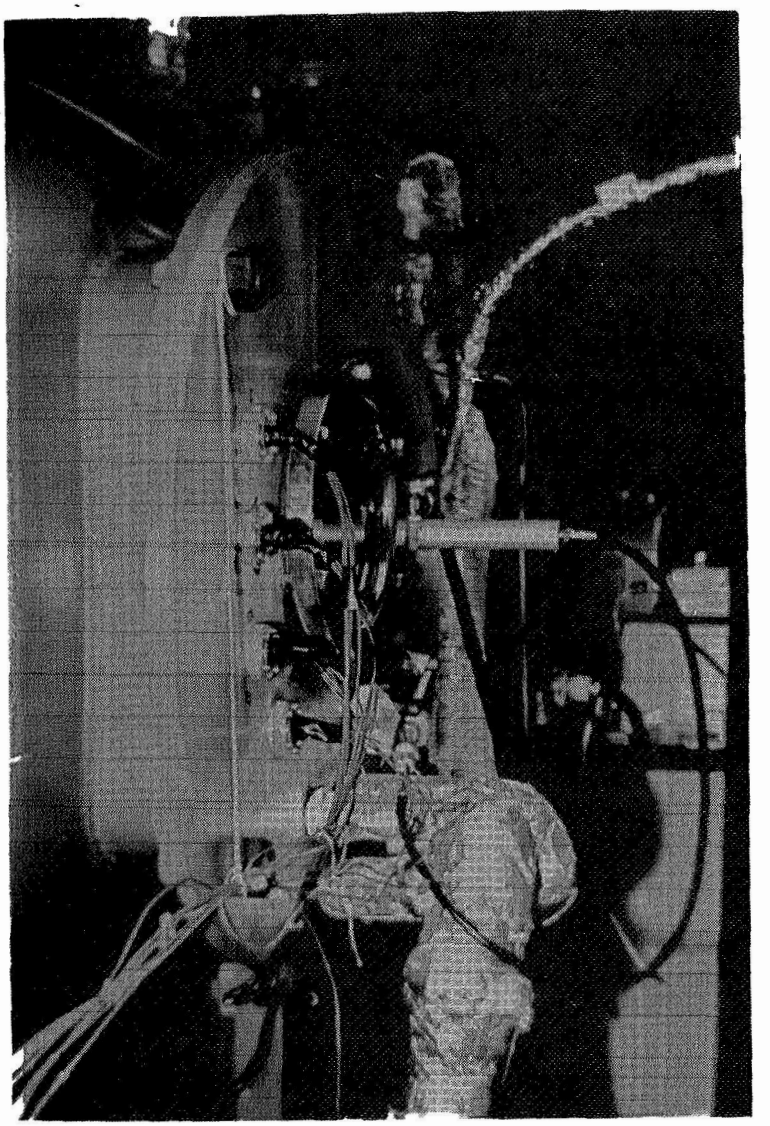

Figure III-2 Flange Plate
and Feedthroughs

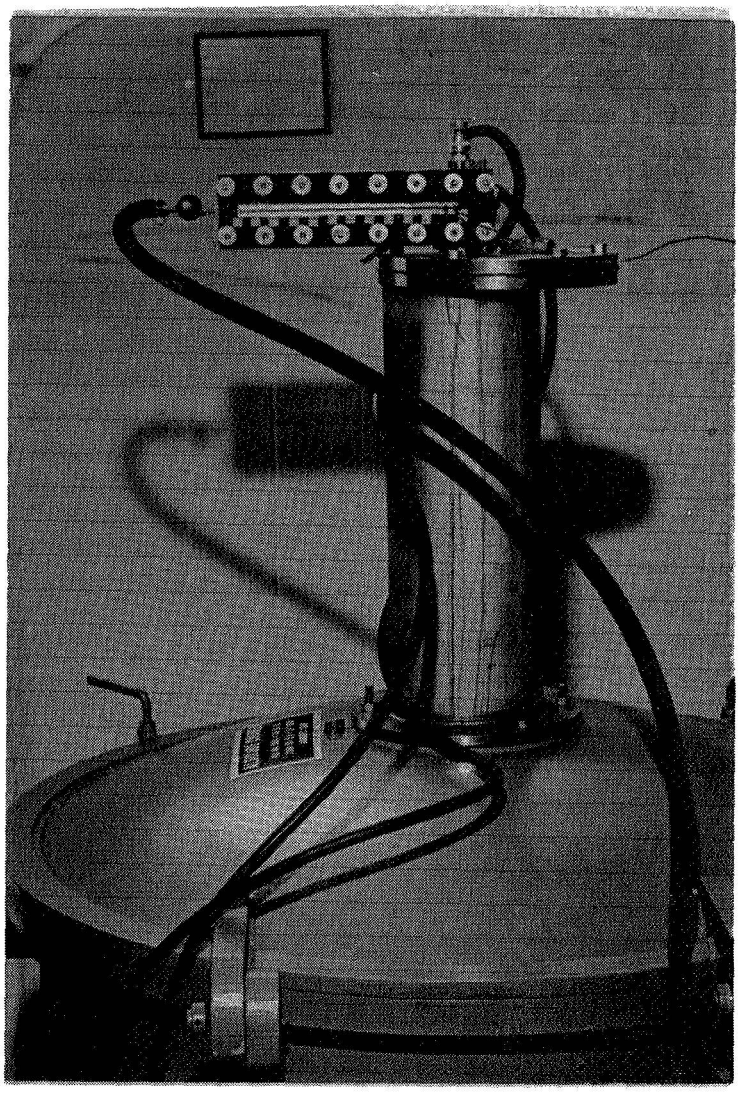

Figure III-4 Chamber Extension and Fluid Injection System

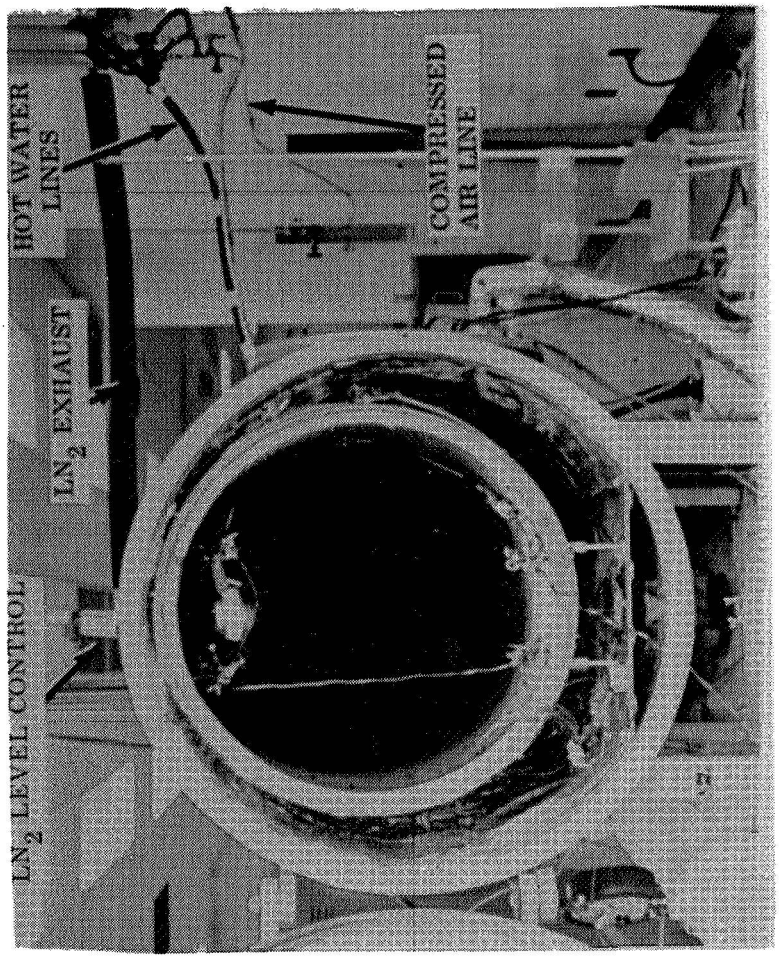

Figure III-3 End View of Cryogenic Liner

necessary to place a cylindrically shaped liner (Figure III-3) within the chamber. Wrapped around and connected to the liner is 5/8 inch copper tubing in which the liquid nitrogen (LN_2) is circulated. A temperature of approximately $160^{o}R$ was sensed by two copper-constantan thermocouples connected to the liner. A Nextel Velvet Coating 101-C10 black paint was applied to the inside of the liner to simulate the black conditions of a space environment. Three circular holes were cut in the liner to correspond with the viewing ports.

An additional modification was made to the chamber to allow the venting of a fluid into the vacuum. The glass viewing port on the door of the chamber was removed and replaced by a cylindrical (10 inch diameter by 24 inches long) extension. The fluid injection system (Figure III-4) was sealed to the open end of the extension. The injection system basically consisted of a liter tank to hold the water, a valved pressurization line, a plunger for starting and stopping the fluid flow, a threaded hole for a nozzle, a hot water line to heat the nozzle to prevent freezing, and a thermocouple placed in the tank to measure the water temperature before injection. The modifications to the vacuum chamber were performed primarily by Mr. Steddum.

A special sample holding and protection device (Figure III-5) was constructed to be used during testing. It was necessary to have three samples in the chamber during a single pump down because of the length of time required to pump down the chamber to space conditions and then return it to atmospheric conditions. Two 1/8 inch stainless steel plates were cut in the shape of a 4-1/2 inch by 22 inch rectangle. In the center of each plate, a 2-7/8 inch square hole was cut to expose

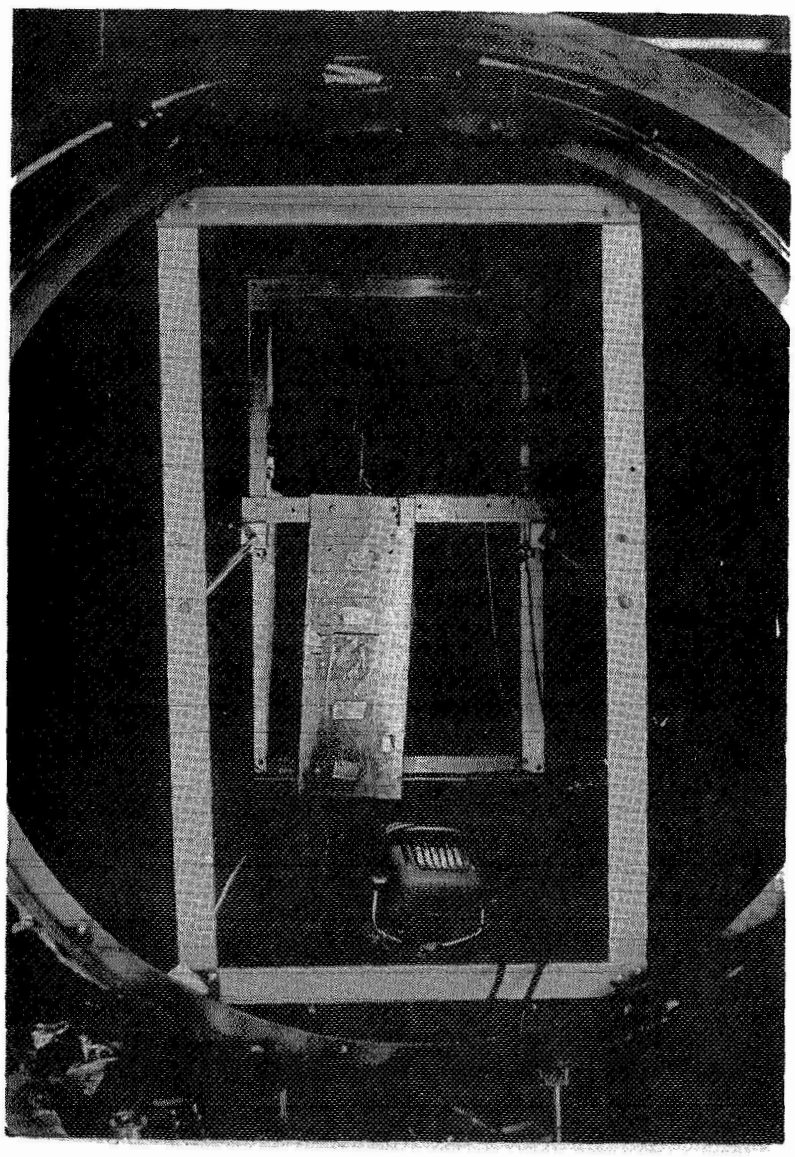

Figure III-5 Multiple Sample Holding Device

a single sample to the water jet while the other two samples were protected by the plates. One of the holes was cut to allow the back of the exposed sample to be irradiated by a variable high temperature heater. The two stainless steel plates were separated by 1/4 inch aluminum spacers. The spacers were bolted to the plates at a distance from one another sufficient to allow the samples to freely slide in the holding device. A pulley system was used to move the samples into place during the testing. The mechanical feedthrough provided the rotary motion to operate the system. The sample protection device was attached to the movable plate assembly used in Mr. Steddum's investigation.

The water spray was photographed with a model WF-148 Wollensak Fastex "S" high speed camera. The most successful pictures were taken at approximately 7000 frames per second with a 35mm focal length lens at f 2.8 using Ektachrome B 16mm color film. A single 3 x 3 inch sample was held in the rear of the chamber with a clamp attached to a ring stand. Floodlights were placed directly above and below the sample. This particular positioning of lights allowed the water spray to be viewed before and after the sample was struck. The intensity of the floodlights was controlled with a variable transformer that allowed the proper color temperature for photographing. The Fastex camera pictured the sample from a viewing port located at the rear of the chamber (Figure III-1). Positioning the camera at this port facilitated clear photography of the spray as it impinged on the sample's surface.

Monochormatic Light Source

A Beckman Model DU Spectrophotometer was modified to provide a monochromatic light source. The monochromator is a single pass quartz

prism type. The original tungsten lamp was replaced by a xenon lamp source. Because of this change the monochromatic beam was deflected to exit through a side rather than front port. The xenon light source provides greater energy over the wavelength of interest as well as comparing favorably with the Johnson (NRL) curve [2] used to simulate high quality solar radiation. The resulting monochromator provides a wide wavelength range from 200 to 2000 millimicrons. The majority of the sun's energy is emitted within this range. A slit adjustment control is used to increase the intensity of the beam. The slits are continuously adjustable from 0.01 to 2.0 millimeters.

The light beam is directed through a chopper into a light-tight box containing a spherical mirror that changes the path of the beam. The light is focused on a square inch sample placed inside the integrating sphere. The light chopper is a small four-blade fan rotating at 166 cycles per second. The circular 4.25 inch diameter front surface spherical mirror has a 0.81 meter (31.9 inch) radius of curvature and a 0.405 meter (15.95 inch) focal length. The mirror was purchased from Oriel Optics Corporation in Stamford, Connecticut. This firm vacuum deposited Al-SiO on the front surface of the mirror. The mirror was polished to a 1/4 of a wavelength.

To prevent extraneous light from entering the sphere, a light-tight box, consisting of a frame covered by black polyethlene, was fabricated. The monochromatic beam entered the box through a 2 x 4 inch rectangular opening in the polyethylene. To insure the fact that only the monochromatic beam entered the sphere, the exposed portion of the sphere was protected by an overlapping polyethylene sheet attached to the light-tight box. As added protection, room lights were extinguished when measurements were being made. A schematic of the measuring system

and an overall view of the apparatus is shown in Figures III-6 and III-7.

Integrating Sphere

Two spheres, obtained from the Weber Brass Company of Cleveland, Ohio, were used in the construction of the integrating spheres. One of the spheres consisted of two hemispheres of 6 inch radius with a 1/2 inch flange and the other was of two hemispheres of 4 inch radius with a 1/2 inch flange. The hemispheres were spun from aluminum to a thickness of 0.04 inches and were bolted together to form 12 and 8 inch diameter spheres. Four holes were cut in the spheres, two for the detectors, one for the sample holder and another to allow the light to enter. The detector openings were cut 50^{o} on each side of a vertical plane passing through the center of the sphere and 50^{o} below a horizontal plane also passing through the center. These detector openings were cut into the sphere at these angles to prevent the incoming beam from being directly incident on the detectors regardless of whether the sample was in or out of the light's path. The monochromatic beam entered the sphere through a one inch diameter hole cut to coincide with a line formed by two intersecting planes passing through the center of the sphere. This positioned the opening directly opposite the detectors. Ninety degrees above the entrance opening a two inch diameter hole was cut for the sample holder.

The first sample holder designed and used with the 12 inch sphere was inadequate. Vibrations encountered when the sample was moved in and out of the beam's path caused flaking of the MgO coating. The improved sample holder (Figure III-8) used with the 8 inch sphere consisted of

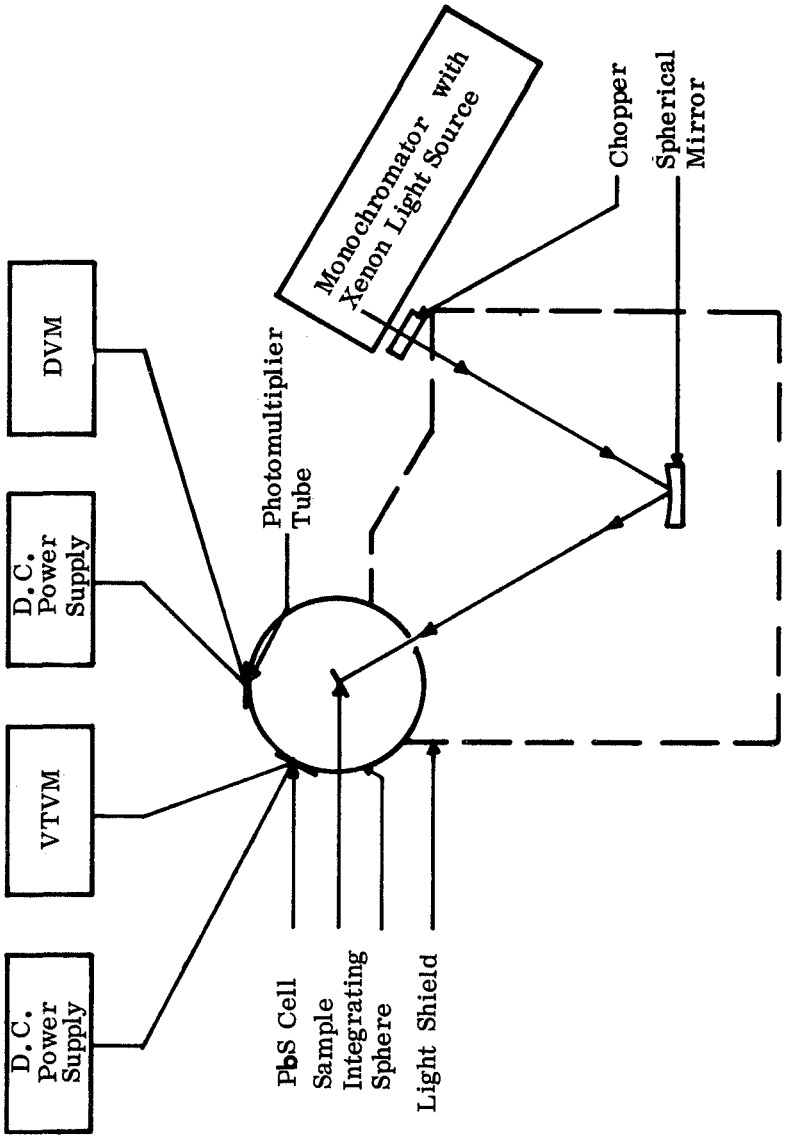

Figure III-6 Schemetic of Reflectance Measuring System

Figure III-7 Overall View of
Measuring System

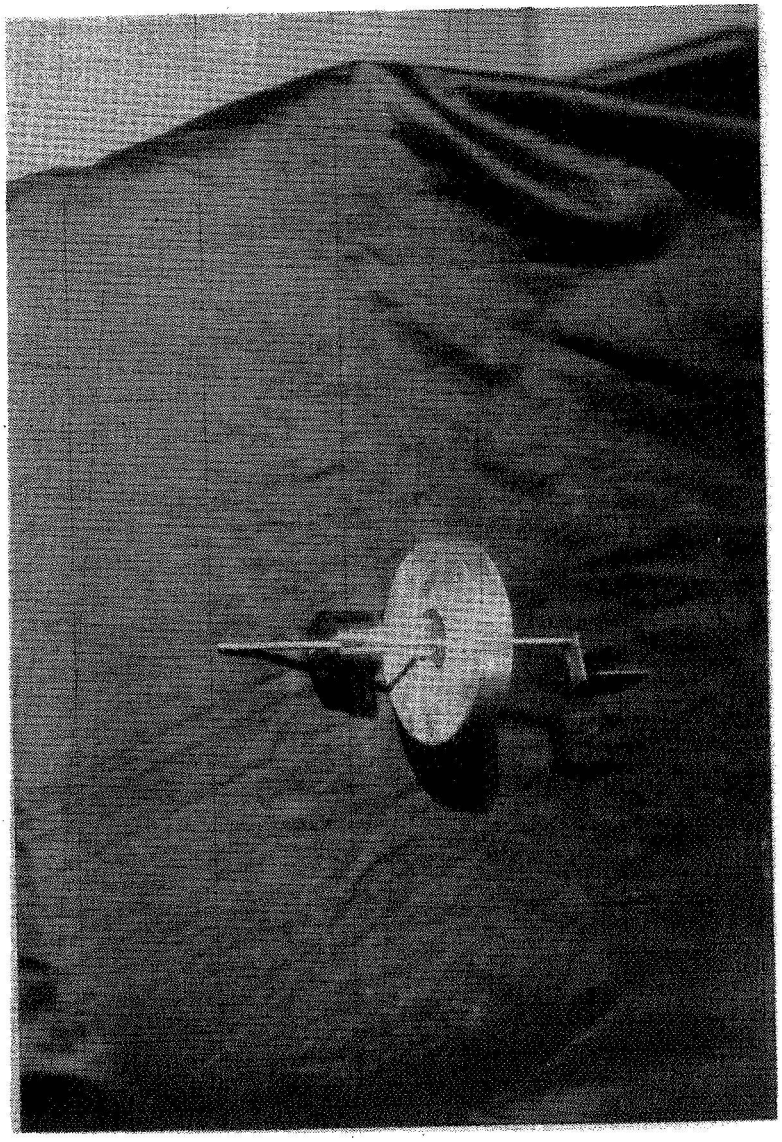

Figure III-8 Sample Holder

three parts. The base of the sample holder was machined from a 3 inch circular piece of 5/8 inch thick aluminum. One side of the base was cut so it would fit snugly against the sphere while maintaining the spherical inside geometry. On the flat side of the base a one-inch circular, 1/4 inch groove was cut. In the center a hole was drilled to permit the insertion of a 1/8 inch rod. A 1/32 inch stainless steel plate was tack welded to the bottom of the rod, providing a place to attach the test samples. A collar was also machined to provide easy circular motion when positioned in the groove. A set screw, drilled and tapped in the collar, was used to fasten the rod at the point necessary to position the sample in the center of the sphere.

The inner wall of the sphere and that portion of the sample holder within the sphere were coated with magnesium oxide (MgO). Two methods of applying the oxide were examined. Initially, a 6000 volt D.C. potential was placed between the hemisphere and a piece of mesh wire. This method resulted in uniform coverage of the surface, but the texture was rough and not acceptable. Coating the surface by the smoking technique was found to be the more effective approach. This was done by holding magnesium stripping with a pair of needle-nose pliers and setting it on fire. The main disadvantage of hand smoking is the difficulty in obtaining a uniform coating. To combat this problem an equal amount of magnesium stripping was applied to the hemispheres. The hemispheres were divided into five equal sections, a top section and four equal quadrants. Each section was smoked with identical amounts of magnesium. An estimate of 1-1/2 to 2 millimeters of magnesium oxide covered the interior of the two hemispheres. The one exception of the coating thickness occurred at the junction of the hemispheres. To minimize flaking when the

hemispheres were bolted together, a thinner coating was applied near the flanges.

After the sphere was coated, it was placed on the top of a rectangular plywood box (Figure III-9). The lower portion of the sphere to which the detectors were attached was placed inside the box. This positioning prevented the detectors from sensing stray light, but permitted the monochromatic beam to enter the sphere.

Detection and Recording Systems

Due to the small amounts of energy available for detection in the ultraviolet and near-infrared regions, one criteria for selecting a detector was that it possess a maximum degree of sensitivity. Another consideration was that the detectors fit as flush against the sphere as possible. With these two considerations in mind, two types of detectors were selected.

A 1P28 RCA photomultiplier tube was used as a detector in the range of 250 to 700 millimicrons and a lead sulfide (PbS) cell for wavelengths greater than 700 millimicrons. The photomultiplier tube is a nine stage side-on type with an S-5 spectral response. The photocathode, which is the light sensing element, is approximately 0.31 inches by 0.94 inches. The hole cut into the sphere was slightly larger and made it possible for the photocathode to view the inner surface of the sphere. The tube was surrounded by foam rubber and taped to the sphere as shown in Figure III-10. A 10mm by 10mm lead sulfide cell was purchased from Optoelectronics in San Rafael, California. It was mounted on a vector board and similarly taped to the sphere.

To supply the necessary voltage to operate the detectors, two D.C.

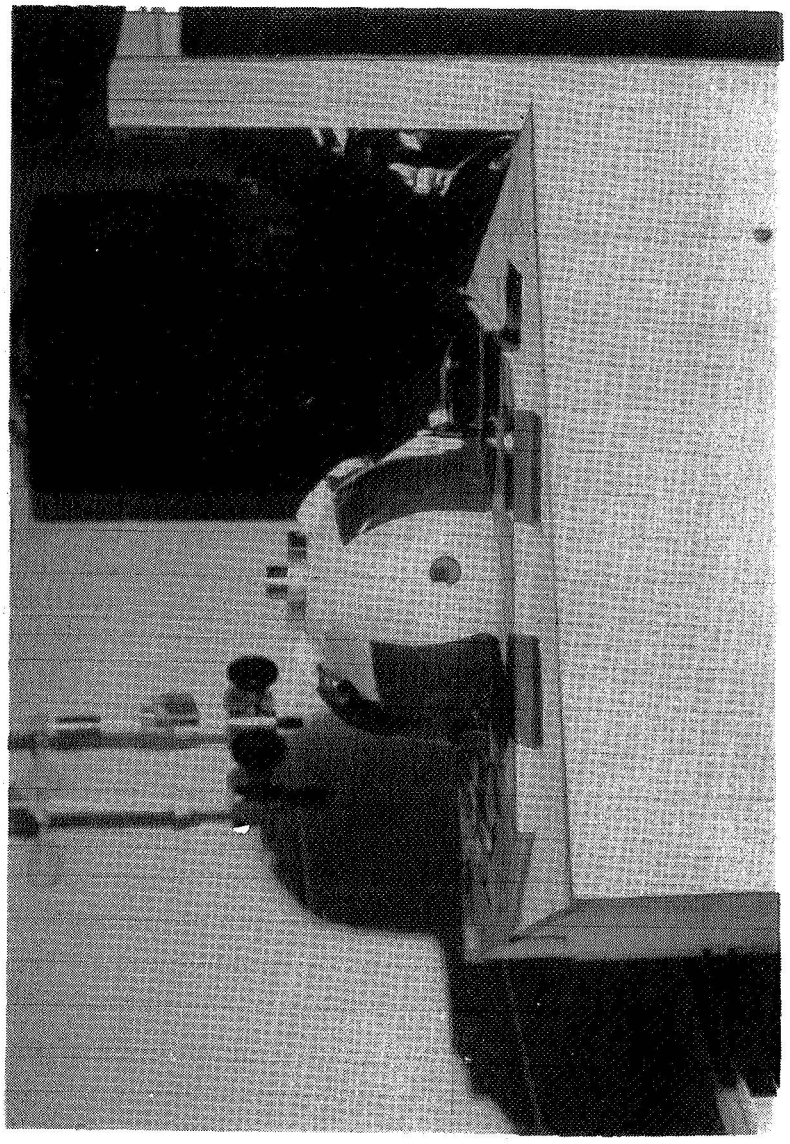

Figure III-9 Eight-inch Integrating Sphere

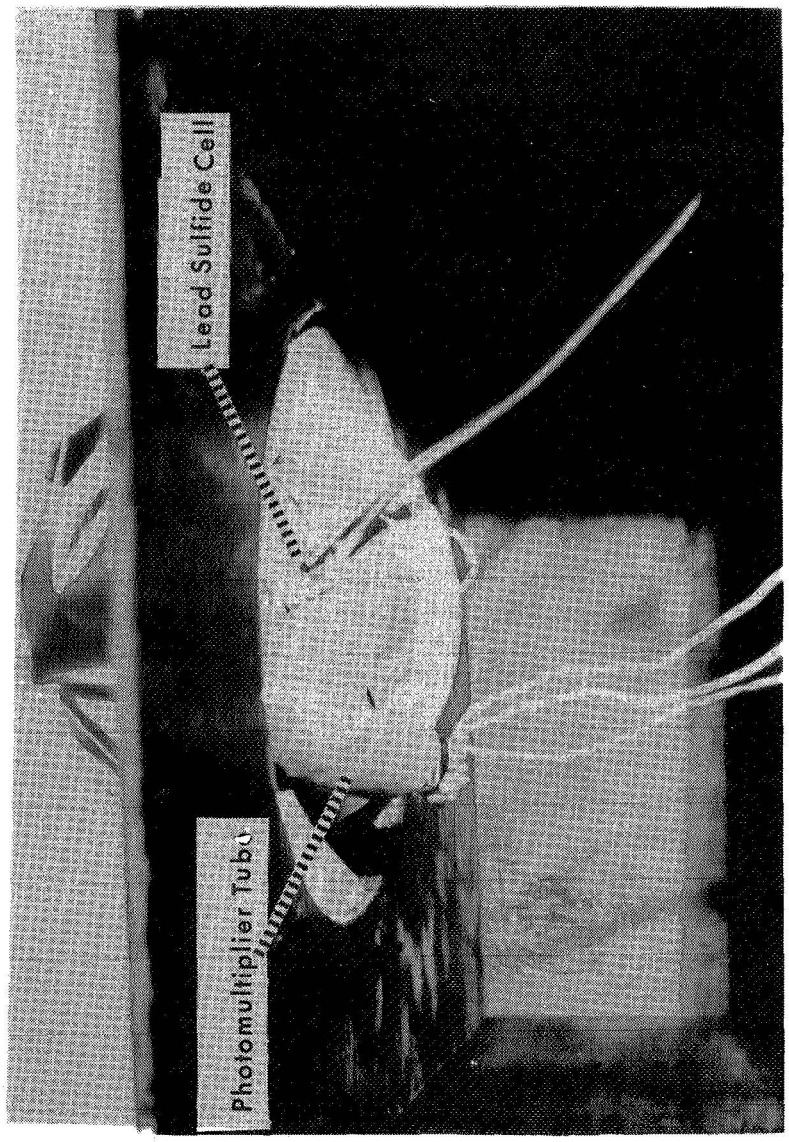

Figure III-10 Detectors Attached to Integrating Sphere

power suppliers were used. The photomultiplier tube requires a 1000 volt D.C. potential to operate at its peak efficiency. A 200 volt D.C. potential was placed across the lead sulfide cell. The supply voltage apparatus is shown in Figure III-11.

The electrical outputs of the detectors are read on a Vacuum Tube Voltmeter (VTVM) and a Digital Voltmeter (DVM). The manufacturer recommended that for best response of the PbS cell an alternating signal should be used. Chopping the light source resulted in an A.C. output which was read on a VTVM. D.C. output was read from the photomultiplier tube. The voltage drop across a 20K ohm load resistor was used to detect the average amount of light per unit area within the sphere. This voltage drop was put initially on a strip chart recorder. Due to the difficulty in the continuous setting of the deflection scale on the recorder, the output was read directly from a digital voltmeter.

Considerable difficulty was encountered in wiring the detection systems. Presented in Figure III-12, are the manufacturers' suggested electrical circuits for both the photomultiplier tube and the lead sulfide cell.

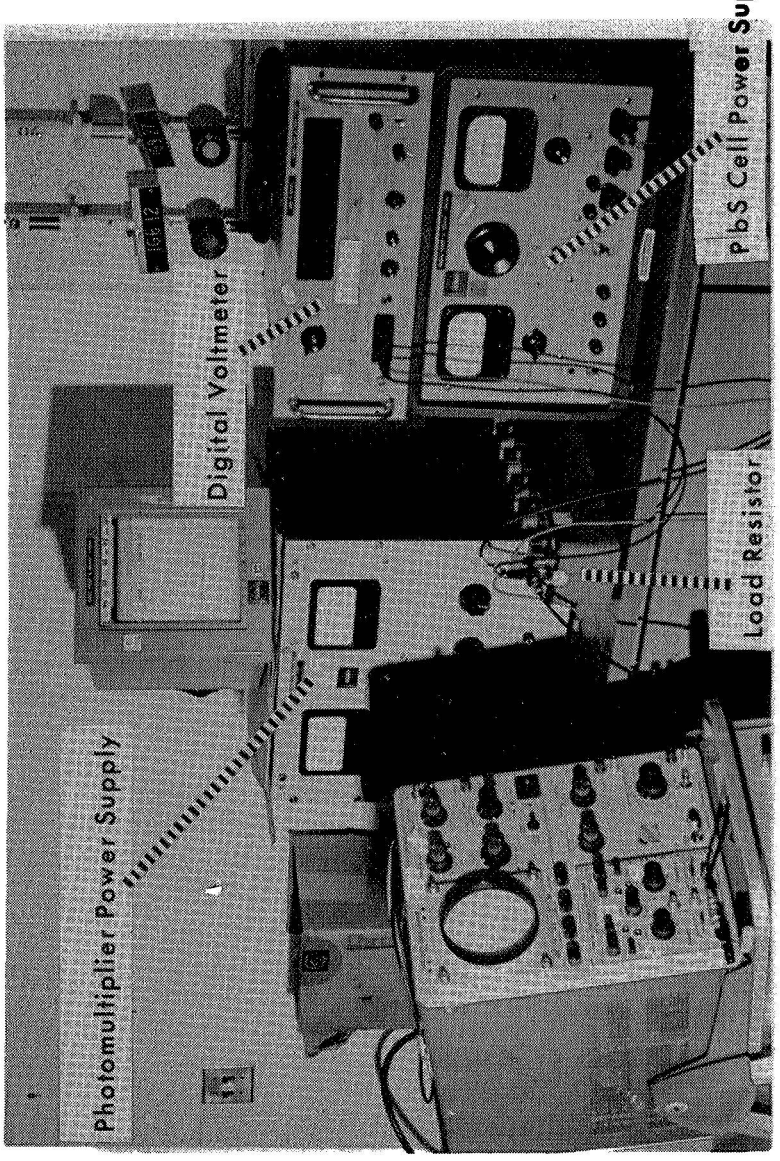

Figure III-11 Power and Recording Equipment

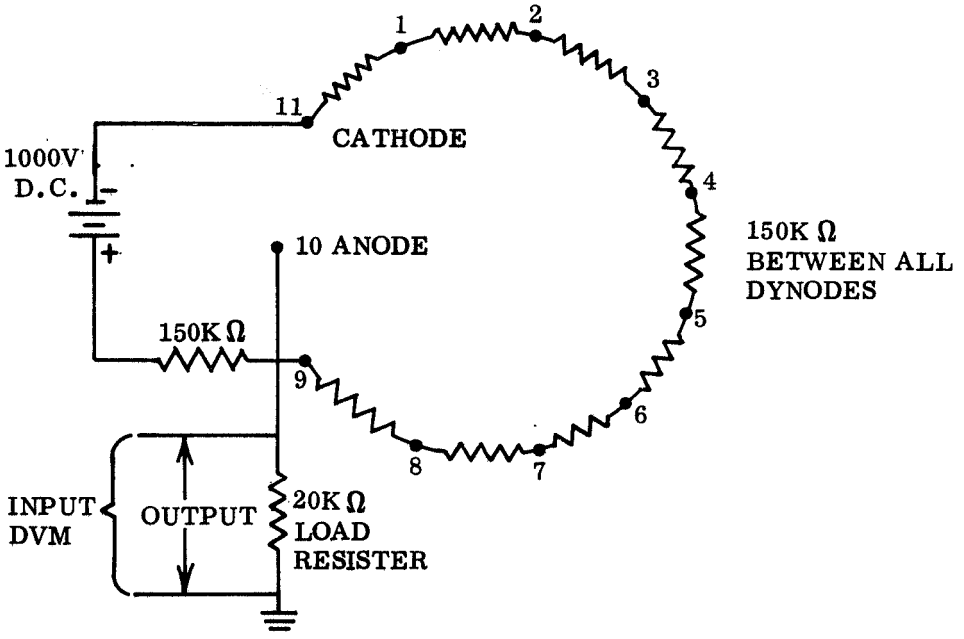

PHOTOMULTIPLIER ELECTRICAL CIRCUIT

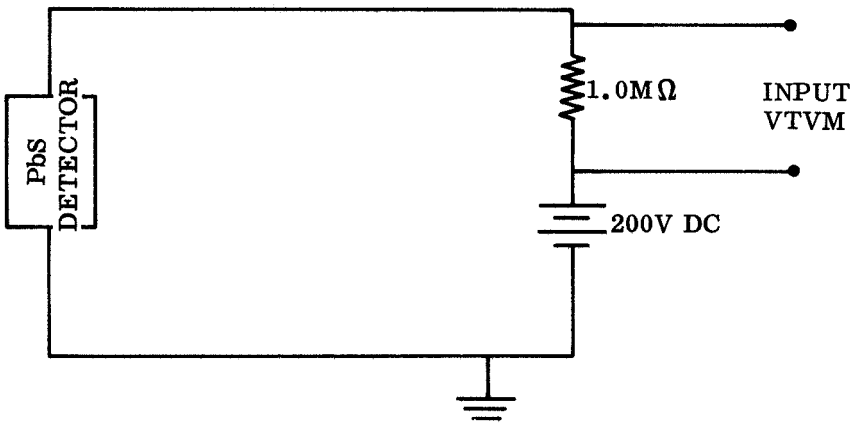

LEAD SULFIDE ELECTRICAL CIRCUIT

Figure III-12 Electrical Circuits for Detection Equipment

CHAPTER IV

EXPERIMENTAL PROCEDURE AND RESULTS

Test Samples

The prime consideration for the selection of paints to be tested was their ability to withstand variable temperatures and extremely low pressures while maintaining their physical properties. The thermally-controlled paints applied to spacecraft best fulfilled these requirements. Three different paints, Z93 and S13G being used on the SIVB, the proposed space workshop, and Dow Corning 92-007, a backup for S13G, were chosen for study. The SIVB paints were selected because of their high spectral reflectance values. Since reflectivity is related to surface conditions, it was believed that a greater chance for degradation would occur with these paints. An additional reason for their selection was that these paints, applied to the entire exterior of the Apollo Telescope Mount (ATM) and solar cell arrays in the back of the workshop, were in a likely position to be struck if venting of excess water became necessary.

All paint samples were obtained from Mr. King, head of the Materials Group at NASA Marshall Space Flight Center. Due to extreme difficulty in applying these paints, Mr. King's group prepared and applied the paints to 6 x 6 inch aluminum plates. Also obtained from Mr. King were the data on the spectral responses of these paints.

The Z93 is a zinc oxide pigmented potassium silicate paint [4]. The paint is prepared immediately before use and is applied by spray.

The coating is porous and relatively soft and can be cleaned with a detergent and water. A thickness of 5 mils yields a minimum solar absorptance (α_s) of 0.15. The paint has good stability in a space environment showing only an increase of 0.014 in absorptance after 4200 earth sun hours (ESH).

S-13G [4] is a zinc oxide pigmented silicone paint. The paint is rubbery and resilient and should be cleaned with a water moistened clean, soft cloth. A primer is used to increase its adherence to metal substrates. The minimal solar absorptance of 0.19 is obtained at a thickness of nearly 10 mils. The solar absorptance increased 0.06 when the paint was subjected to 2400 ESH. The Dow Corning 92-007 commercial paint is also a silicone paint. The paint is rubbery and tends to spring back into its original shape after deformation. Dirt tends to cling to its surface, but it can be cleaned with a moistened clean cloth. Its surface is very smooth, but has the highest value of solar absorptance of 0.22.

Additional testing was performed on aluminum foil taped to stainless steel plates. The reason for this test was because of the obvious surface damage observed by Mr. Steddum.

Exposure Techniques

Information obtained from Mr. Steddum's dissertation [8] on particle velocities and sizes as a function of injection pressure aided the author in selecting the nozzle diameter and injection pressure to be used in this research. The 0.031 inch diameter nozzle was chosen because of the good spray characteristics as compared to the other nozzles tested. The 0.031 inch diameter nozzle was approximately the middle of the range

of nozzle diameters studied. The proper injection pressure was dependent upon two factors. First, it was necessary to provide maximum time for the water droplets to freeze and, secondly, to give sufficient momentum to the particles to insure that they would reach the back of the chamber. If the particles did not contain enough momentum, they would fall to the bottom of the chamber due to gravity before striking the sample. On the other hand, if the injection pressure was too high, the water droplets would not have sufficient time to freeze before striking the sample because of their high velocity. A few tests were made with the sample in the rear of the chamber (74 inches from the nozzle) to determine the proper injection pressure. The pressure finally decided upon was standard atmospheric pressure (14.7 psia).

With the injection pressure and nozzle diameter determined, other decisions to be made were the amount of distilled water to be used on each sample, temperature of water before injection, and the temperature of the sample before impingement. To help in making these decisions, several tests were run on Dow Corning 92-007 paint sample. The 6 x 6 inch plates were cut into four 3 x 3 inch plates. Three paint samples were put in the sample holder with copper-constantan thermocouples attached to the back of the plates.

No heat was applied to the first sample and only one liter of water was used. After injection of a liter of water, the paint sample was covered with a thin coating of ice. Heat was applied to the paint's surface from floodlights placed in the chamber. The intended purpose of the floodlights was to aid in seeing the spray as it struck the sample. The next sample was moved into place. A heater attached to the sample holder, which viewed only the back of the sample, was turned on. The

sample's temperature rose to 90°F before the water was injected. As before, one liter of water was vented into the system and again ice coated the sample at the termination of the test. The heat from the floodlights was used to melt the ice on the second sample before moving the third sample into position. The heater was turned off and the third sample was allowed to stabilize at 42°F. Three liters of water were injected into the chamber. After each liter of water, the injection was stopped and the heater turned on to melt the ice and restore the sample to approximately its original temperature. A drop in plate's temperature of approximately 65°F was recorded after injection of each liter of water.

The samples were taken out of the chamber and visually inspected for damage. No noticeable damage could be seen. A one-inch square was cut from each sample to be used in the 12-inch integrating sphere. Although only spot checks of reflectance values were made, no significant changes in reflectance values were recorded. With this data, the decision was made to apply no external heat to the sample and to reduce the temperature of the injection fluid to a near freezing point.

Ice placed in the fluid injection system lowered the water temperature before injection from 78°F to 34°F. The cold water was injected into the chamber, but icing still occurred on the sample's surface. During this run, aluminum foil was placed directly behind the sample. After three liters of water had been used, the sample was removed and tested for reflectance changes. The results showed no changes had occurred.

Aluminum foil, which had been placed behind the sample, had been heavily damaged. The foil's surface was pitted as if tiny spherical balls had been bombarding it. At this point, a firm decision was made to investigate the effects of the jet on aluminum foil. Three pieces of foil

were taped to 3 x 3 inch stainless steel plates and put in the chamber for testing. The first sample was subjected to the spray for 15 seconds; the second for 30 seconds; and the third for 180 seconds. Figures IV-1 through IV-3 show the damage done to the aluminum foil.

Due to the icing on the paint's surface, it was decided for the next two paint samples high speed motion pictures would be taken of the spray as it struck the surface. A S13G paint sample was placed in the chamber with extra floodlights to illuminate its surface. Two liters of water were discharged into the chamber. The water temperature was 78^{o}F. The reflectance of the S13G paint sample was measured with no significant change being noted. Nothing could be determined about the freezing of the water droplets from the high speed movies taken. The positioning of the lights and camera prevented the particles from being seen as they struck the sample. The camera viewed the sample from the front right port. With the camera in this location, the particles could not be tracked. A glare caused by reflection of the floodlights on the sample made it impossible to see the particles as they hit the surface.

The lighting and the camera positioning was changed for the next test. The test sample painted with Z93 was held in the back of the chamber with a clamp connected to a ring stand. The camera lighting was placed directly above and below the sample so as to illuminate the spray rather than the sample's surface. The camera was moved to the left rear port and positioned to focus on a side rather than front view of the sample. The sample was exposed in the same manner as the S13G sample. After the chamber reached atmospheric conditions, the Z93 sample was removed and it was found that there was visible damage to the paint's surface. Figure IV-4 shows a magnified view of the paint before and after exposure. Similar magnified views of Dow Corning 92-007 and S13G

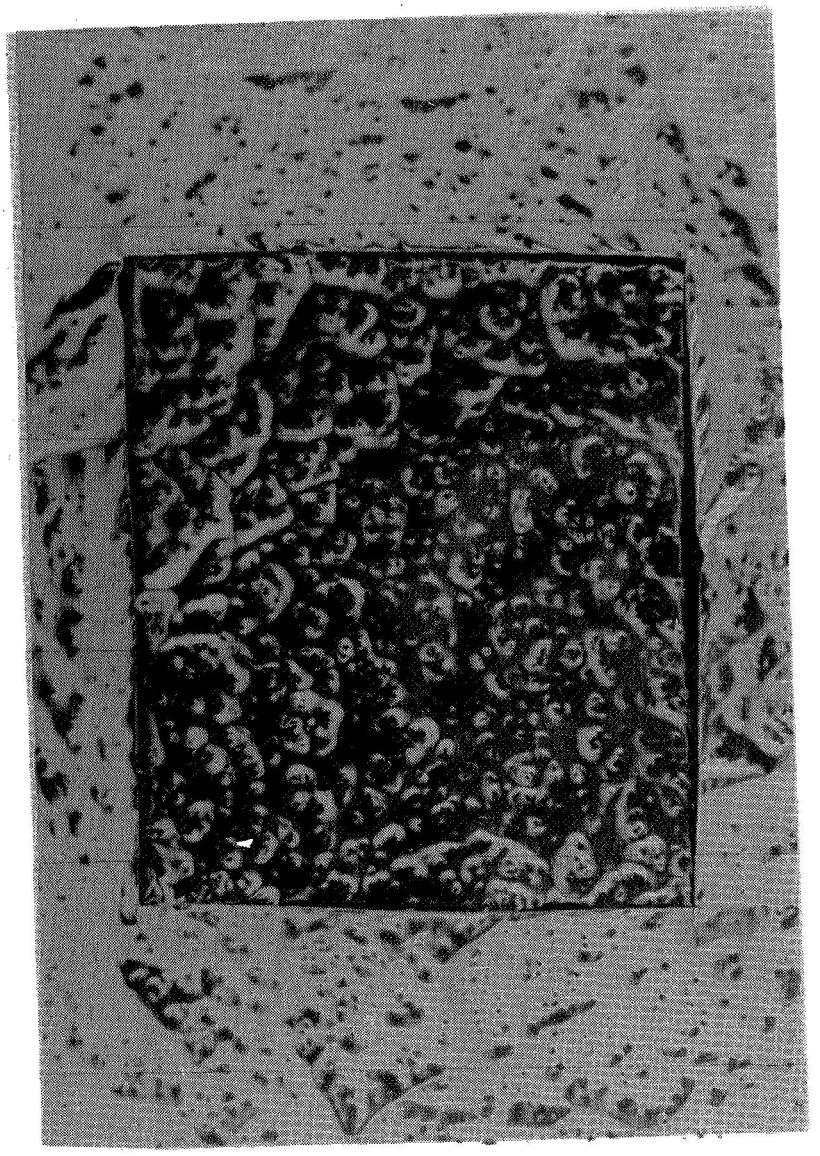

Figure IV-1 Aluminum Foil After 15 Seconds of Exposure to Water Jet

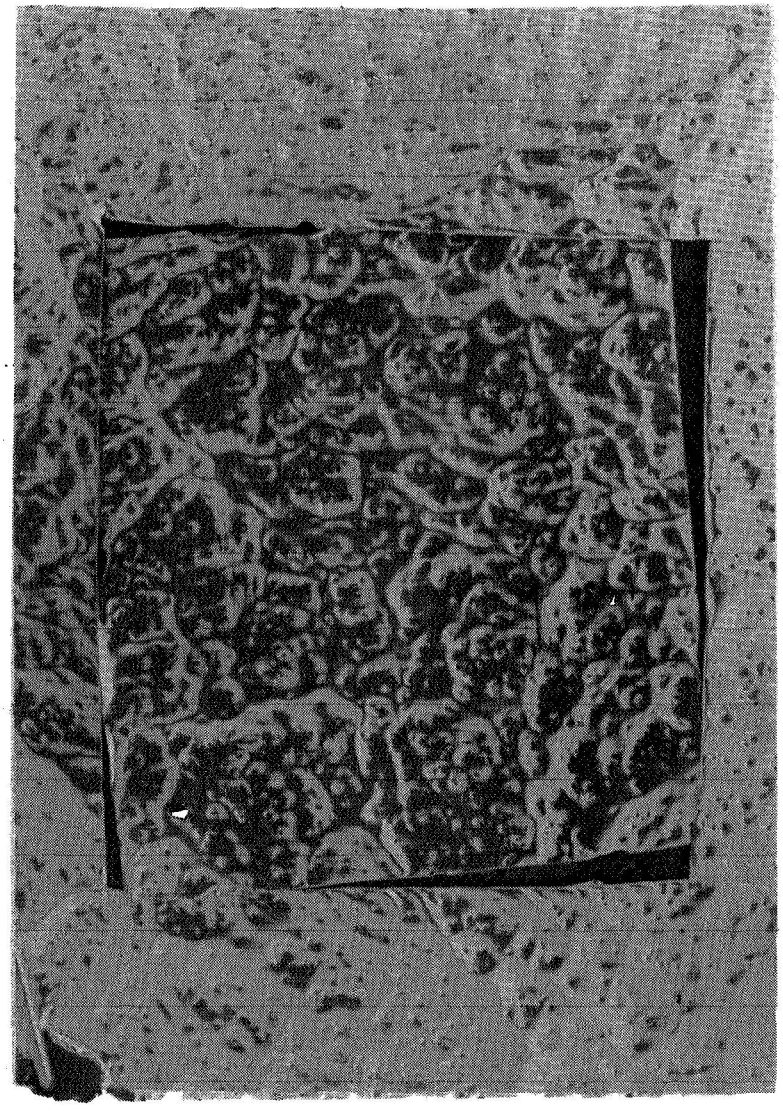

Figure IV-2 Aluminum Foil After 30 Seconds
of Exposure to Water Jet

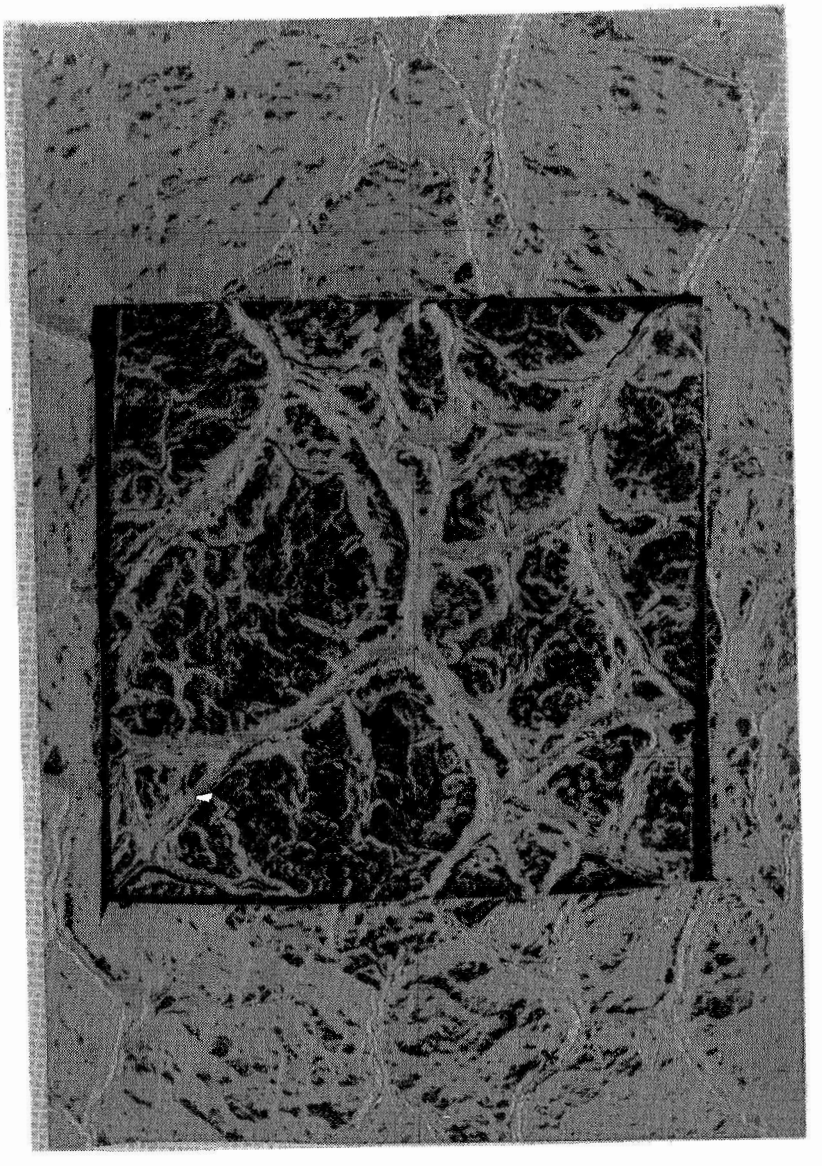

Figure IV-3 Aluminum Foil After 180 Seconds of Exposure to Water Jet

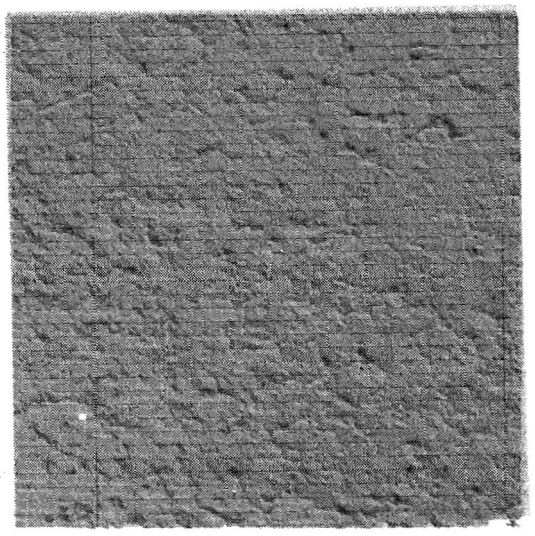

EXPOSED

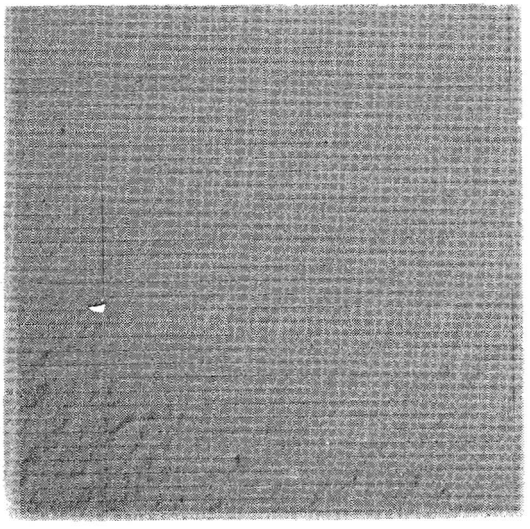

UNEXPOSED

Figure IV-4 Z93 Paint Samples
Before and After Exposure

are shown in Figures IV-5 and IV-6, respectively. Although there was visible damage to the Z93 paint, the reflectometer showed no significant change in reflectance values before and after exposure.

Measurement Techniques

The first sphere used to measure the spectral reflectance of the samples was a 12 inch diameter sphere. A one-inch square was cut from the sample and placed in the sphere. The monochromatic beam was optically aligned and focused on the sample. A 4-1/4 inch diameter spherical mirror having a 45 inch focal length reflected the diverging beam into the sphere. The sample was rotated until the beam was normal to its surface. A pencil mark was made on both the stationary and rotating parts of the sample holder. Fifteen and 90 degree angles measured from the normal were inscribed on the immovable base of the sample holder. To make a reflectance measurement, the sample was rotated 90 degrees from the normal. This allowed the beam to bypass the sample and hit the back of the sphere. With the sample in this position the strip chart deflection scale was placed on 100%. To accomplish this, the slits controlling the intensity of the beam were widened until the deflection needle read full scale. The sample was then rotated into the beam's path 15^{o} past the beam's normal angle of incidence. Due to the absorptance of the sample, the detectors sensed less energy on the sphere's surface which caused the needle to decrease from full scale. This procedure was followed for all the readings recorded from the output of the photomultiplier tube.

At a wavelength of 0.7 microns, the photomultiplier tube output was insufficient to make a measurement. The light chopper was started and the output of the PbS cell was read on a VTVM. When the sample was

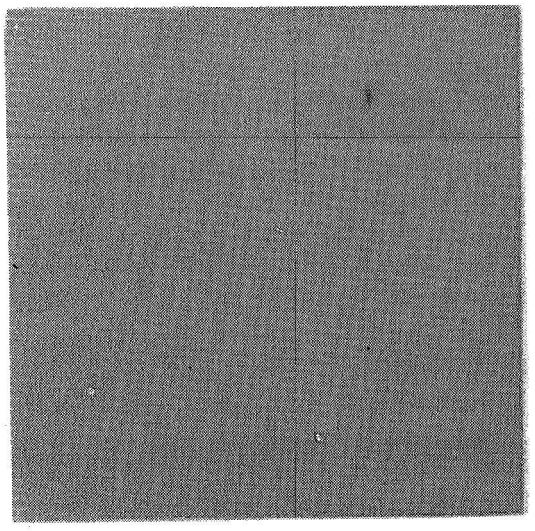

EXPOSED

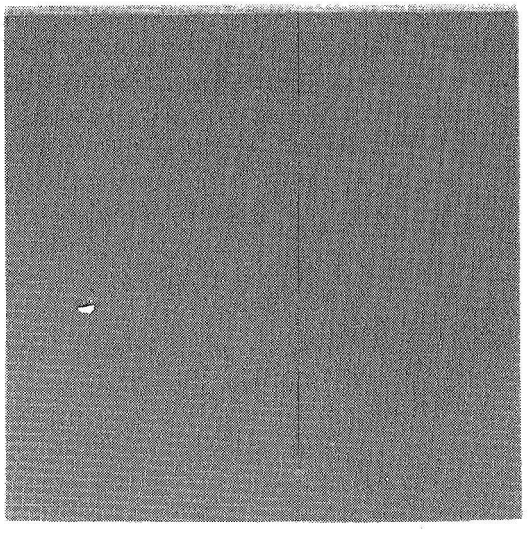

UNEXPOSED

Figure IV-5 Dow Corning 92-007
Paint Samples Before and
After Exposure

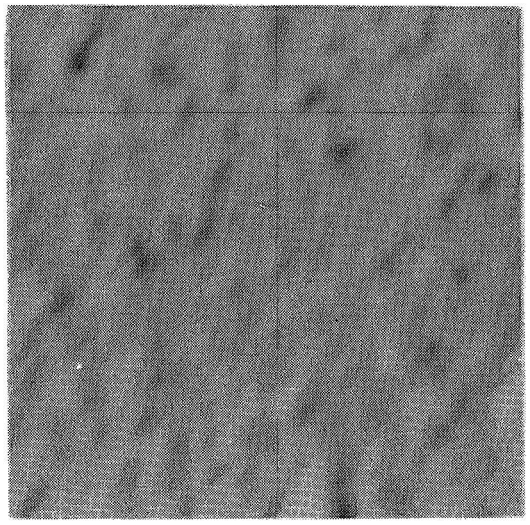

EXPOSED

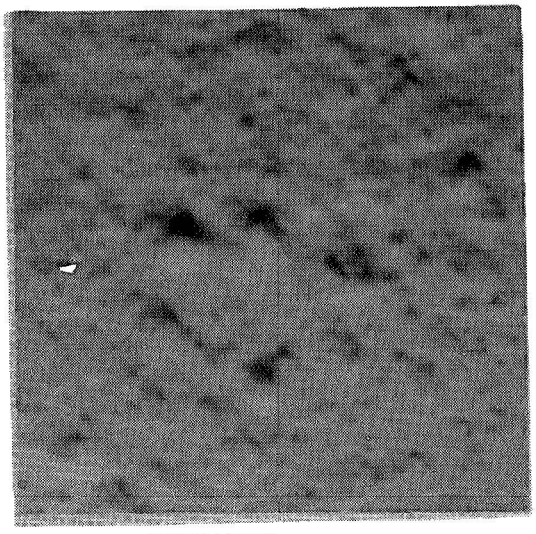

UNEXPOSED

Figure IV-6 S13G Paint Samples
Before and After Exposure

out of the beam's path, the slits were opened until a one millivolt reading was reached. Another reading was taken after the sample was moved into place. The wavelength was incremented in one-tenth micron intervals until 2.0 microns was reached. This incrementation was followed for all the samples measured except when an abrupt change in reflectance was noted. In this case values on either side of the change was measured. Spectral reflectance curves were generated from approximately 30 reflectance values ranging from 0.25 to 2.0 microns.

Results

Reflectance values greater than 100% recorded with the 12-inch diameter sphere made it necessary to redesign the reflectometer. The 12-inch diameter sphere was so designed that the incoming light struck the back of the sphere where the two hemispheres were joined together. At this junction a nonuniformity in the sphere's inner surface was present. The small crack, due to the radius of curvature of the bends to form the 1/2 inch flanges and the insufficient amount of MgO at this junction, resulted in poor reflectance measurements. It is believed that more energy was absorbed in the crack on the first reflectance than the energy absorbed by the sample. To confirm this theory, the sphere was rotated so that the incoming beam was not incident on the crack. Although still high the reflectance values were never above 100% and more closely followed the spectral reflectance data received from NASA.

The location of the sample holder and the entrance opening was switched for the 8-inch diameter sphere. Switching these openings insured that the incoming beam struck a uniform thick coating, resulting in low absorptance on the first reflectance. A change was also made in

the sample holder. The base of the sample holder was changed from a circular to a flat top surface. This change stabilized the sample holder and stopped the coating from flaking off the sample holder. It is believed the flaking was caused from vibrations incurred during rotation of the sample.

Along with the modifications made to the sphere, the data recording system for the photomultiplier was changed. The strip chart recorder was replaced with a digital voltmeter (DVM). Now, rather than setting the deflection needle to 100%, the intensity of the beam was increased until the drop across the load resistor read 100 millivolts. To check the linearity of the phototube, the intensity of the beam was increased to 200 millivolts. The two reflectance values measured were within one-half of a percent of each other. A similar check was made with the PbS cell. Since less energy was needed in the 8-inch diameter sphere to obtain the same output of the larger sphere, the initial setting was increased from 1.0 to 3.0 millivolts. The increase in signal to noise ratio resulted in more accurate measurements. Linearity was established in the PbS cell by increasing the output to 10.0 millivolts and making another reflectance reading.

A comparison of the reflectance values measured with the 12 and 8-inch diameter spheres are shown in Figures IV-7, IV-8 and IV-9. The general shape of the curves are similar, but reflectance values measured with the larger sphere are greater at wavelengths beyond the absorptance edge.

To confirm the accuracy and validity of reflectance values measured with the 8-inch diameter reflectometer, comparisons were made with spectral reflectance data received from NASA. A good comparison for two of the paints (Z93 and S13G) are shown in Figures IV-10 and IV-11.

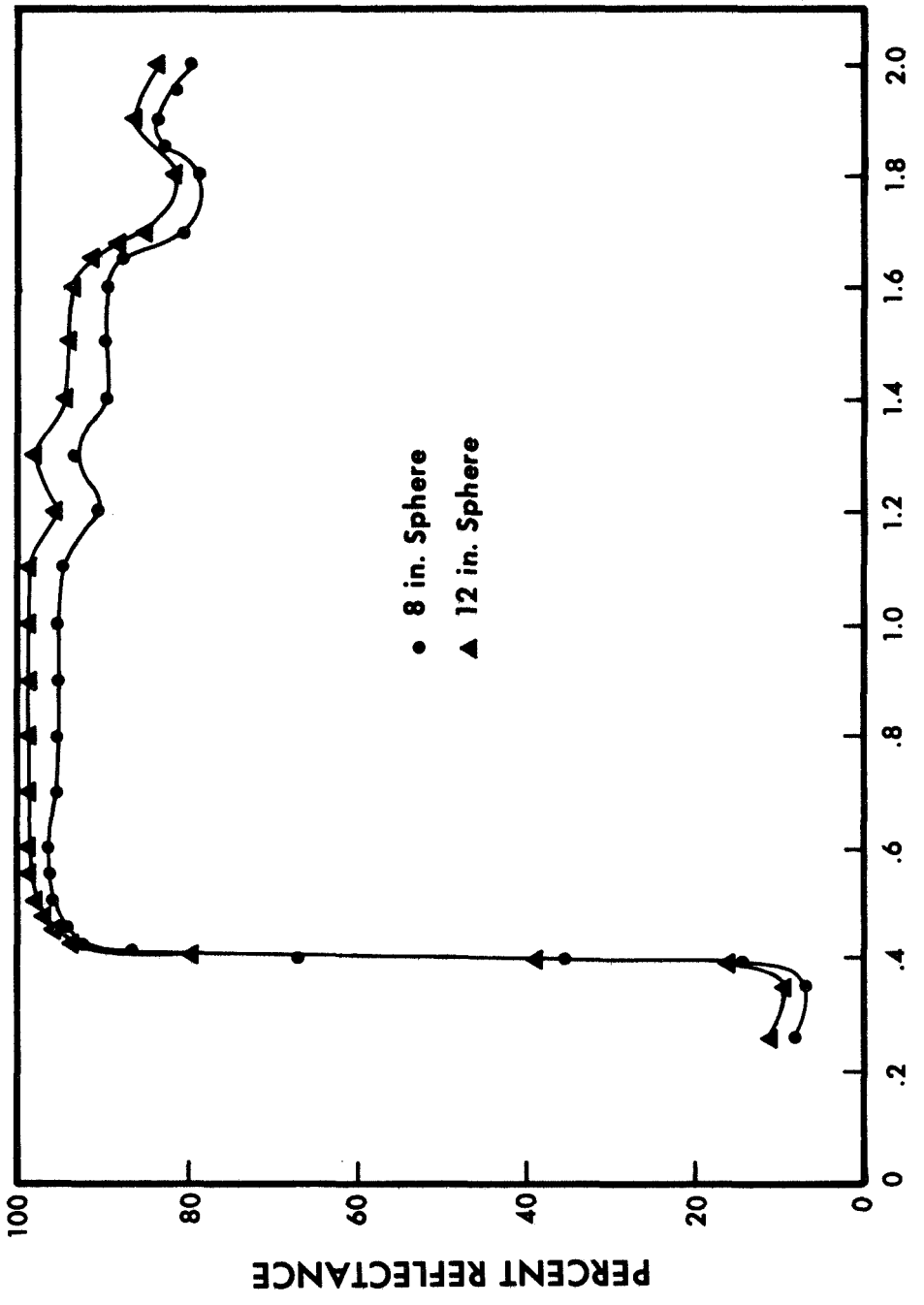

Figure IV-7 Reflectance Data of 92-007 Paint from 8 in. and 12 in. Spheres

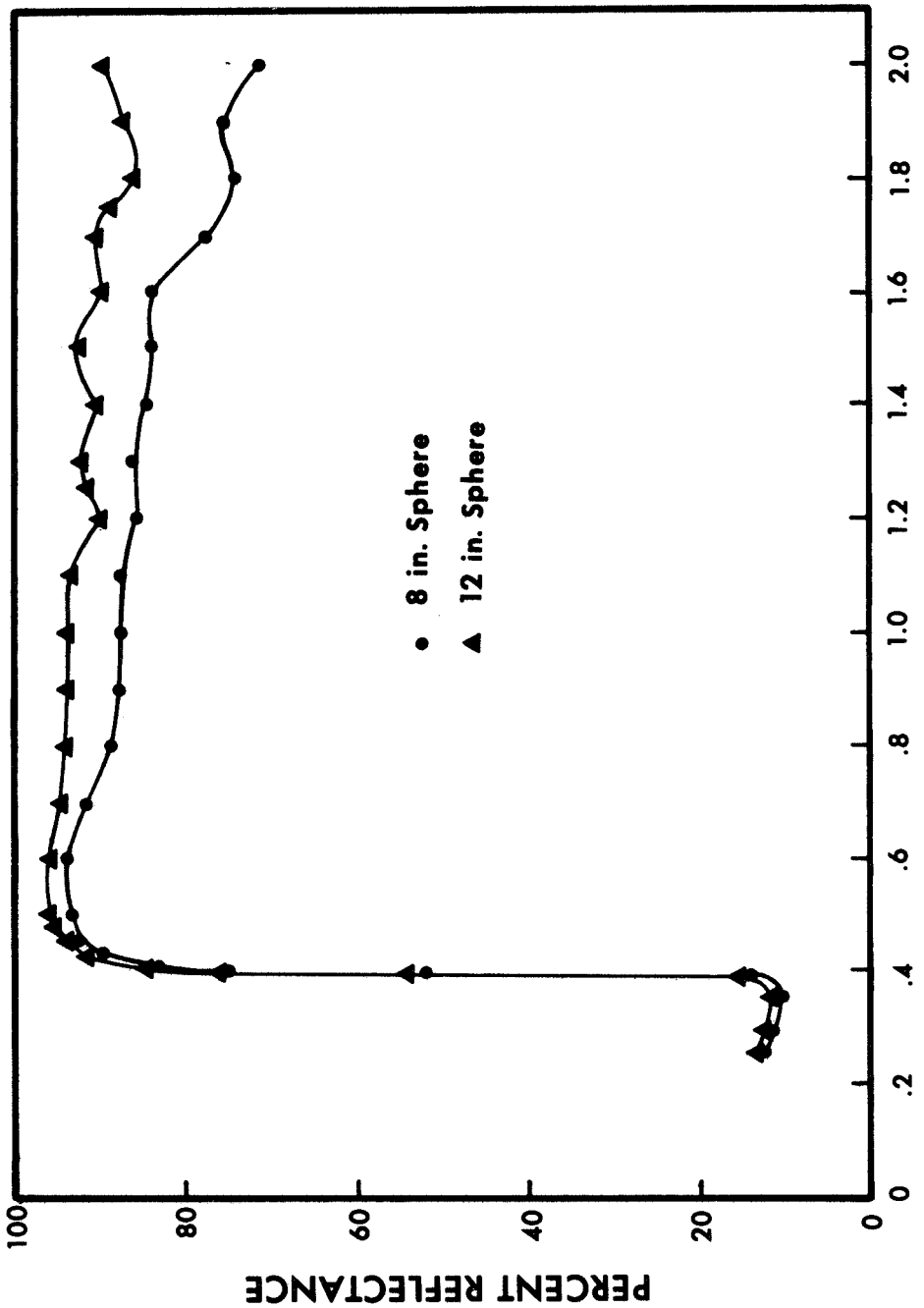

Figure IV-8 Reflectance Data of S13G Paint from 8 in. and 12 in. Spheres

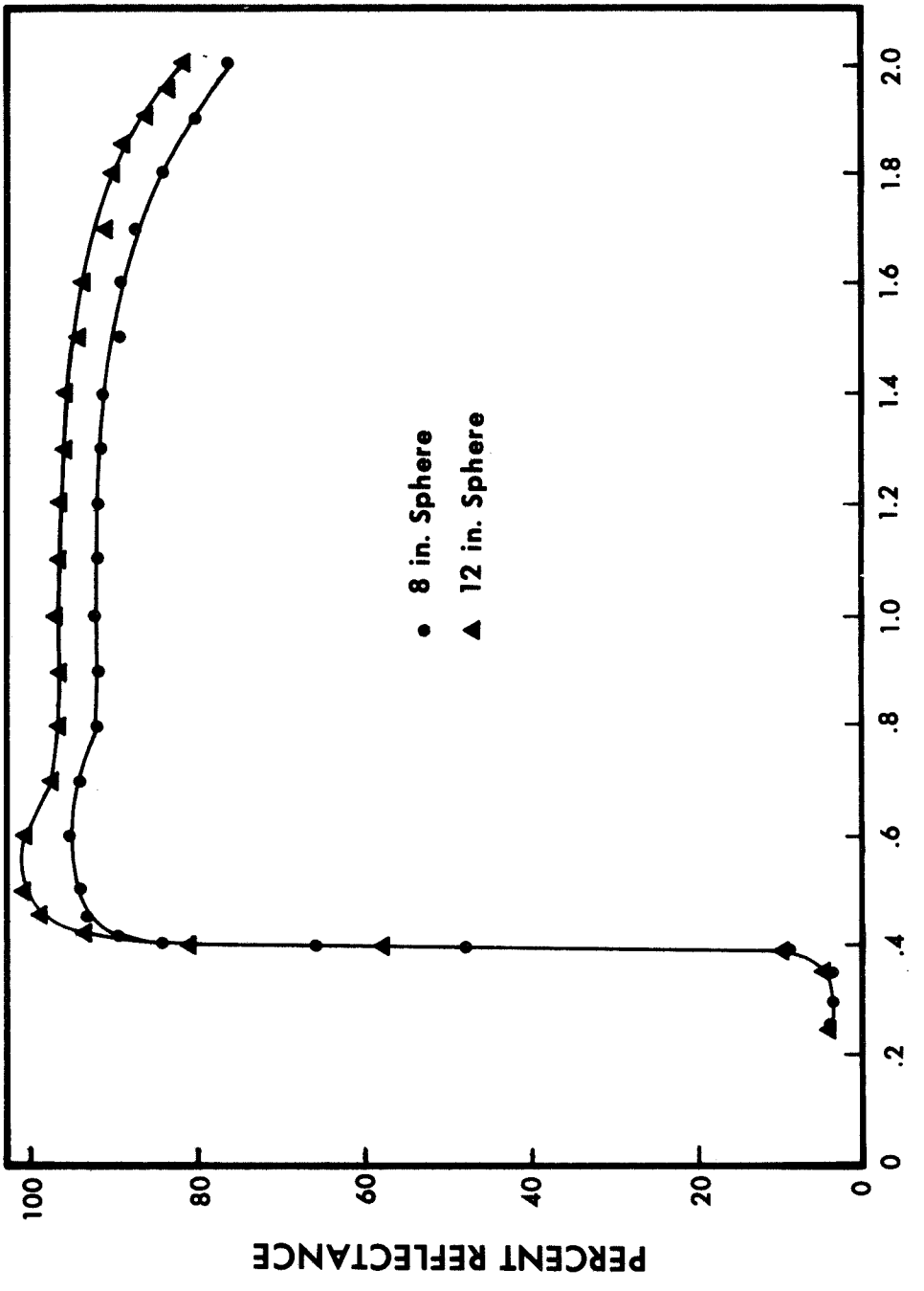

Figure IV-9 Reflectance Data of Z93 Paint from 8 in. and 12 in. Spheres

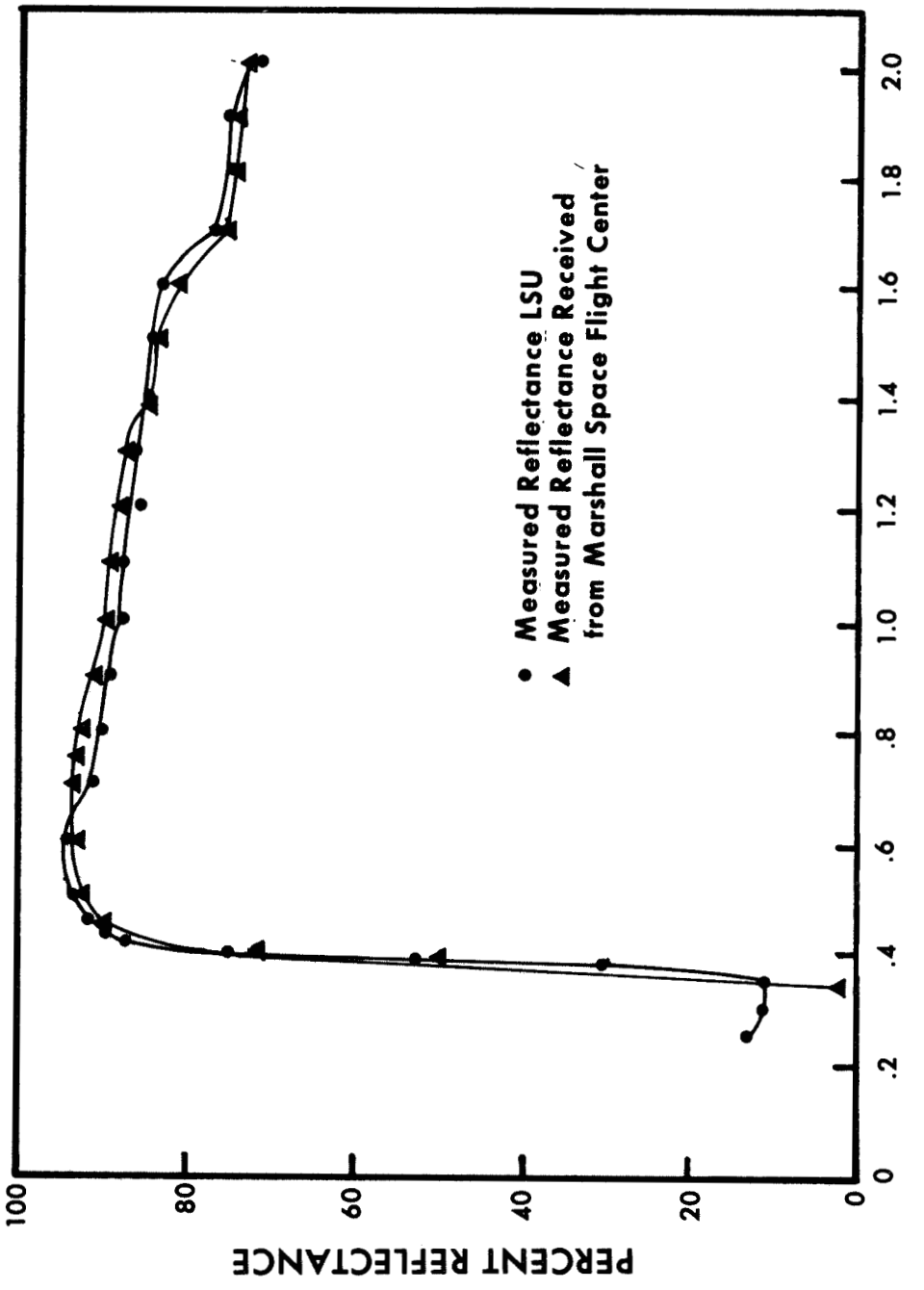

Figure IV-10 Comparison of Reflectance Data for S13G Paint

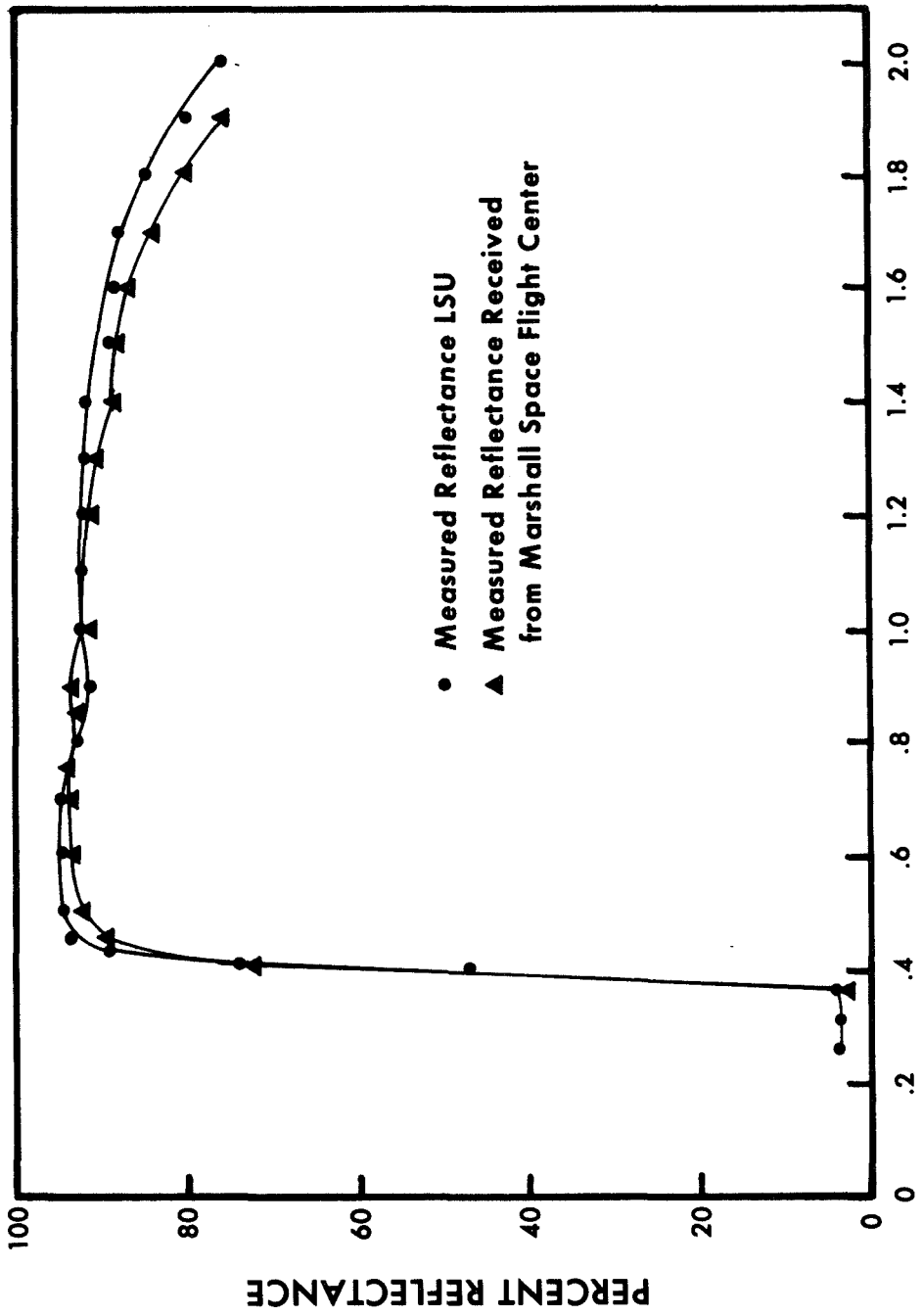

Figure IV-11 Comparison of Reflectance Data for Z93 Paint

However, poor results were obtained for the Dow Corning 92-007 paint (See Figure IV-12). Initially, the problem of why two paints compared favorably and the other unfavorably could not be resolved. It was decided to procure additional data for the 92-007 paint. Fortunately, the author was able to acquire reflectance data on the paint from Dr. J. A. Wiebelt, a professor at Oklahoma State University. The only part of the curve that does not compare adequately occurred from 1.8 to 2.0 microns. In this region, the sphere used in this research showed abrupt changes in reflectance values which resulted in additional measurements. Possibly, if more measurements had been made in this region with Dr. Wiebelt's reflectometer, better comparisons could have been obtained.

It is the author's contention that the data received from NASA is incorrect for only the 92-007 paint. The basis for this belief is that a special measurement of the Dow Corning paint was made by NASA to assist in this investigation. The other two paints spectral responses had been made prior to the beginning of this study. Because of good comparison with Dr. Wiebelt's values, it is thought that some error was made in the special measurement made by NASA on the 92-007 paint.

Convinced that the 8-inch diameter sphere was capable of accurately measuring reflectance values, the exposed samples were remeasured. Presented in Figures IV-13 to IV-15 are reflectance values of the three paints before and after exposure to the spray. All three graphs show no significant changes in reflectance due to the bombardment. In fact, the samples after exposure exhibit slightly higher reflectance values than those prior to exposure.

Plots presented in Figures IV-16 and IV-17 of the aluminum foil show a definite reduction in reflectance values in the longer wavelengths.

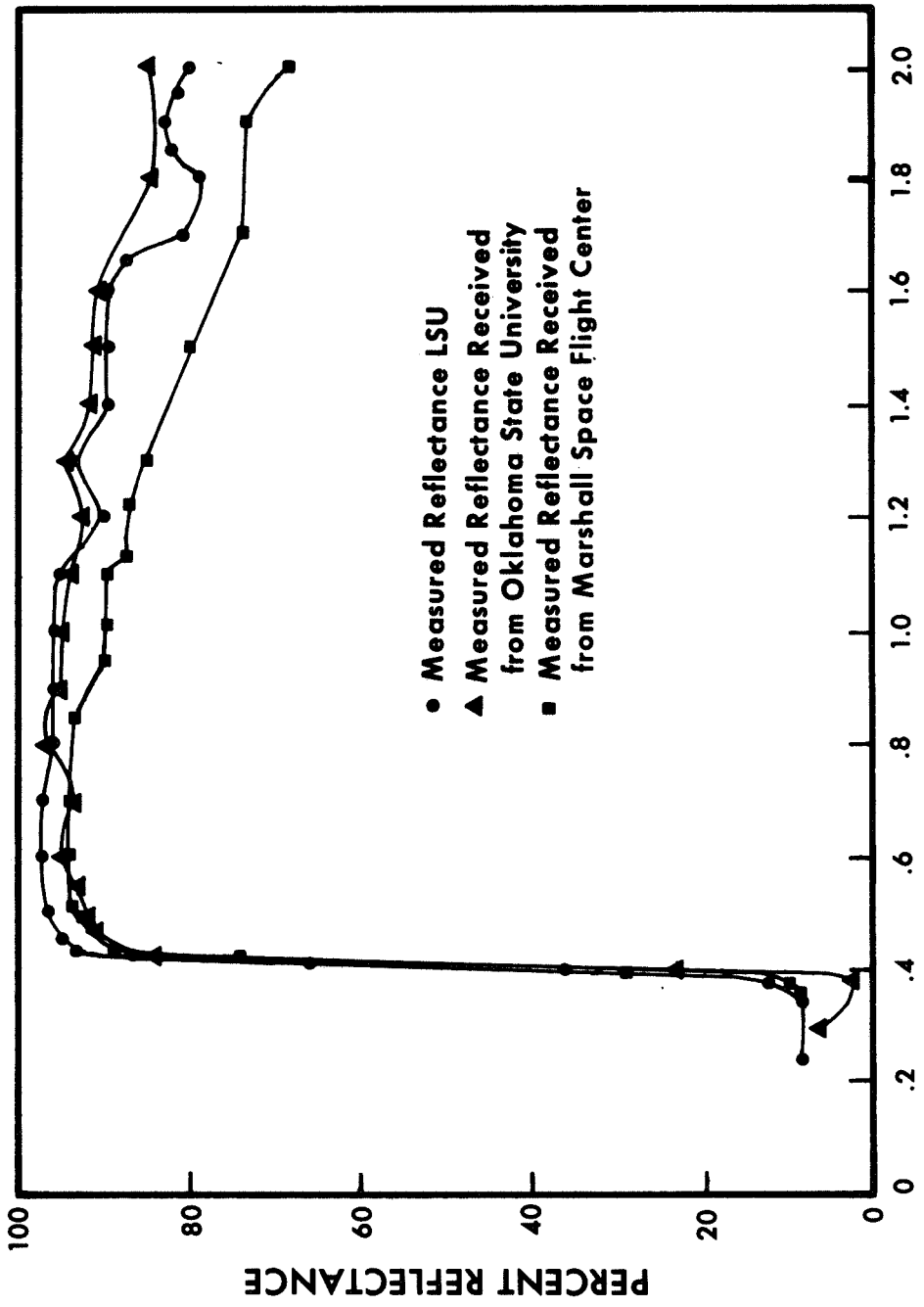

Figure IV-12 Comparison of Reflectance Data for 92-007 Paint

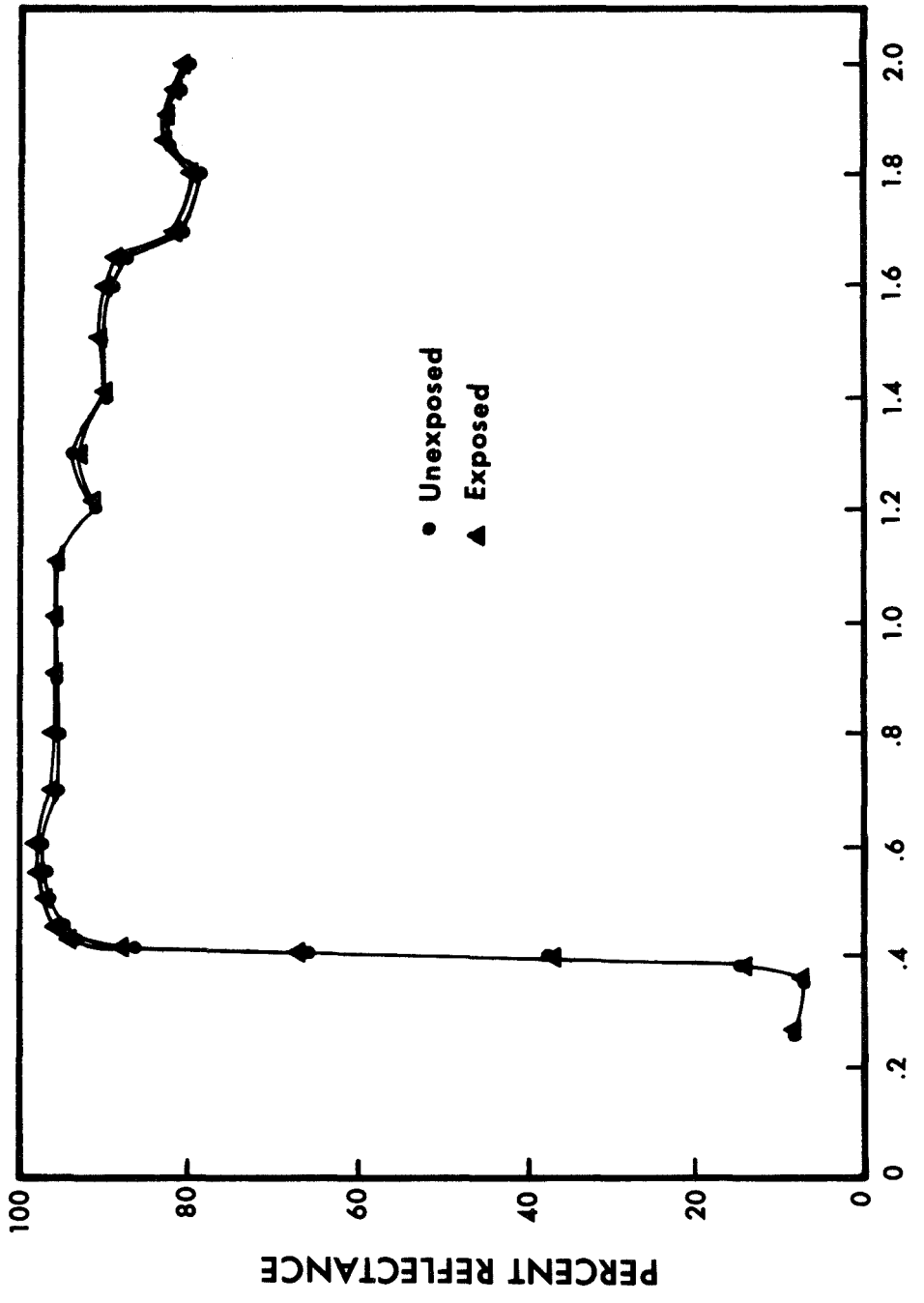

Figure IV-13 Dow Corning 92-007 Paint Before and After Exposure to Water Jet

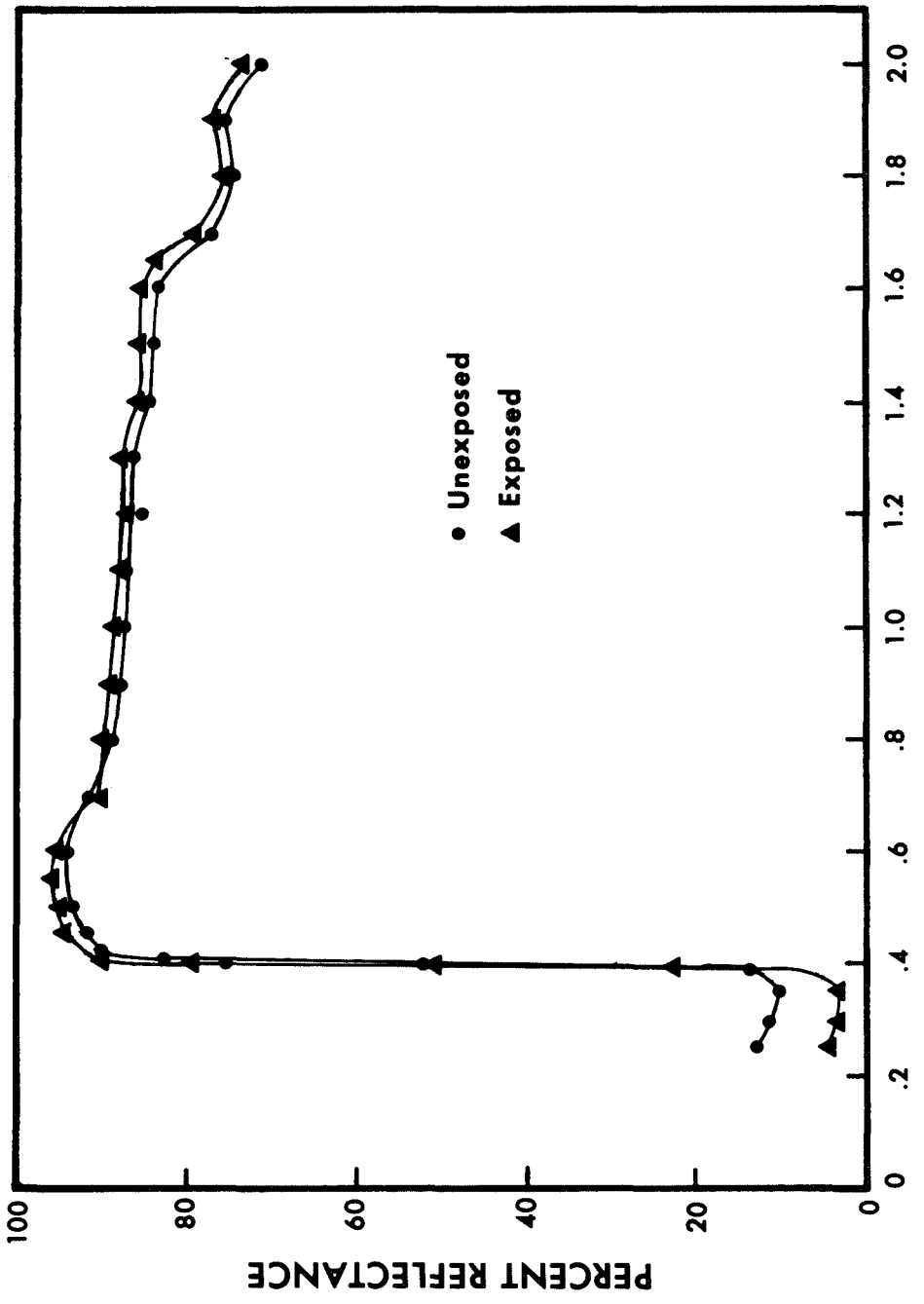

Figure IV-14 S13G Paint Before and After Exposure to Water Jet

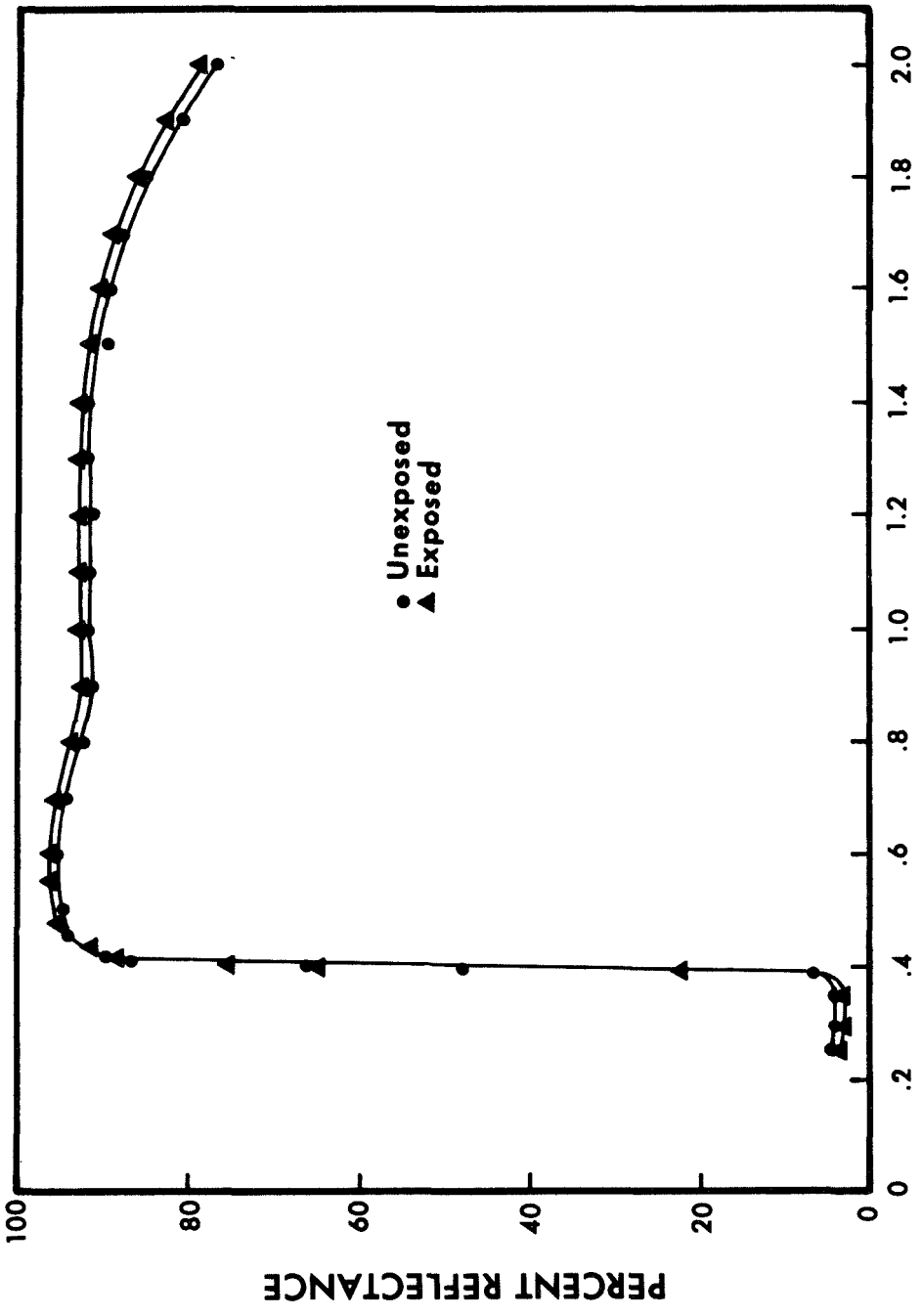

Figure IV-15 Z93 Paint Before and After Exposure to Water Jet

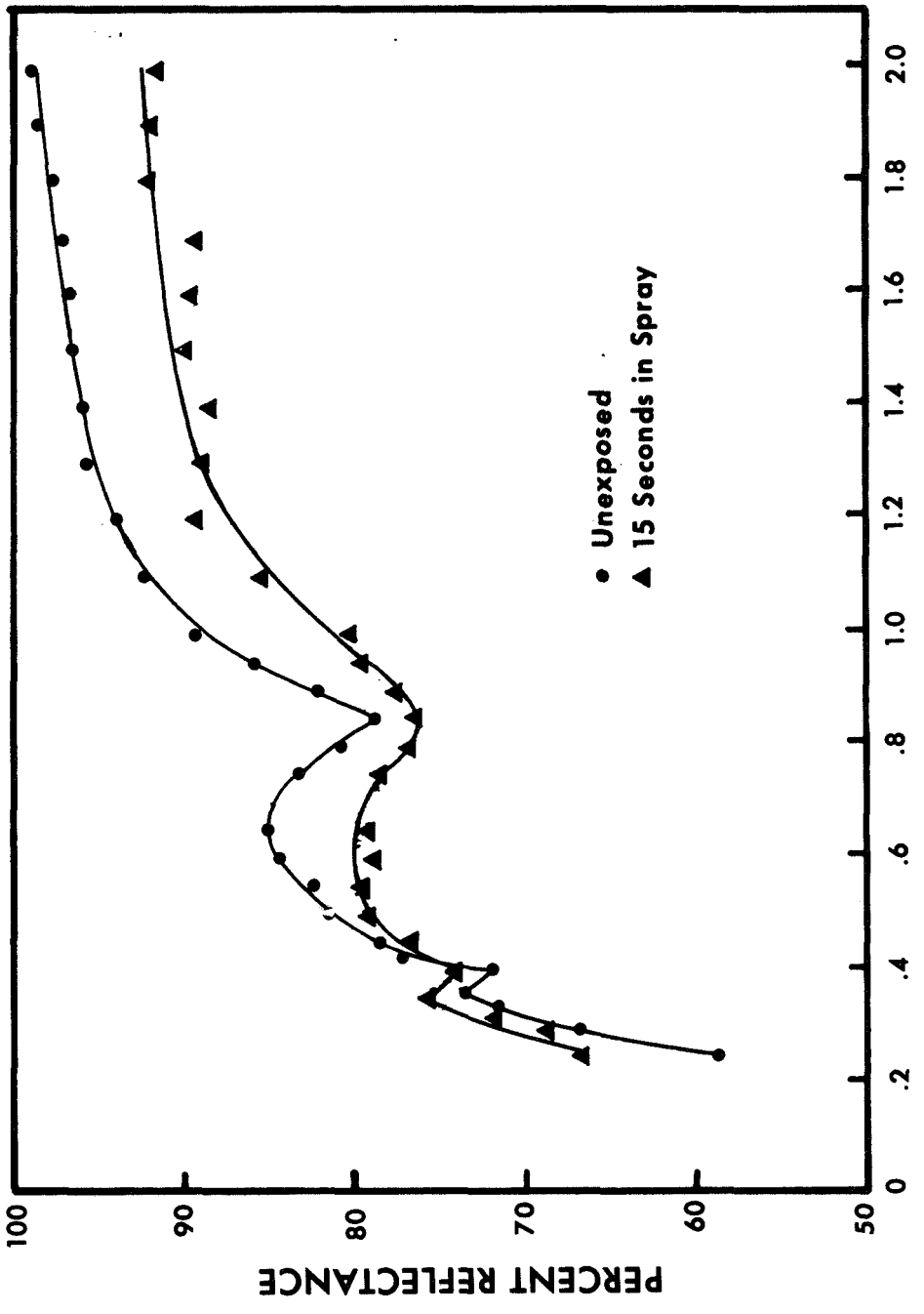

Figure IV-16 Aluminum Foil Reflectance Data (15 Seconds Exposure)

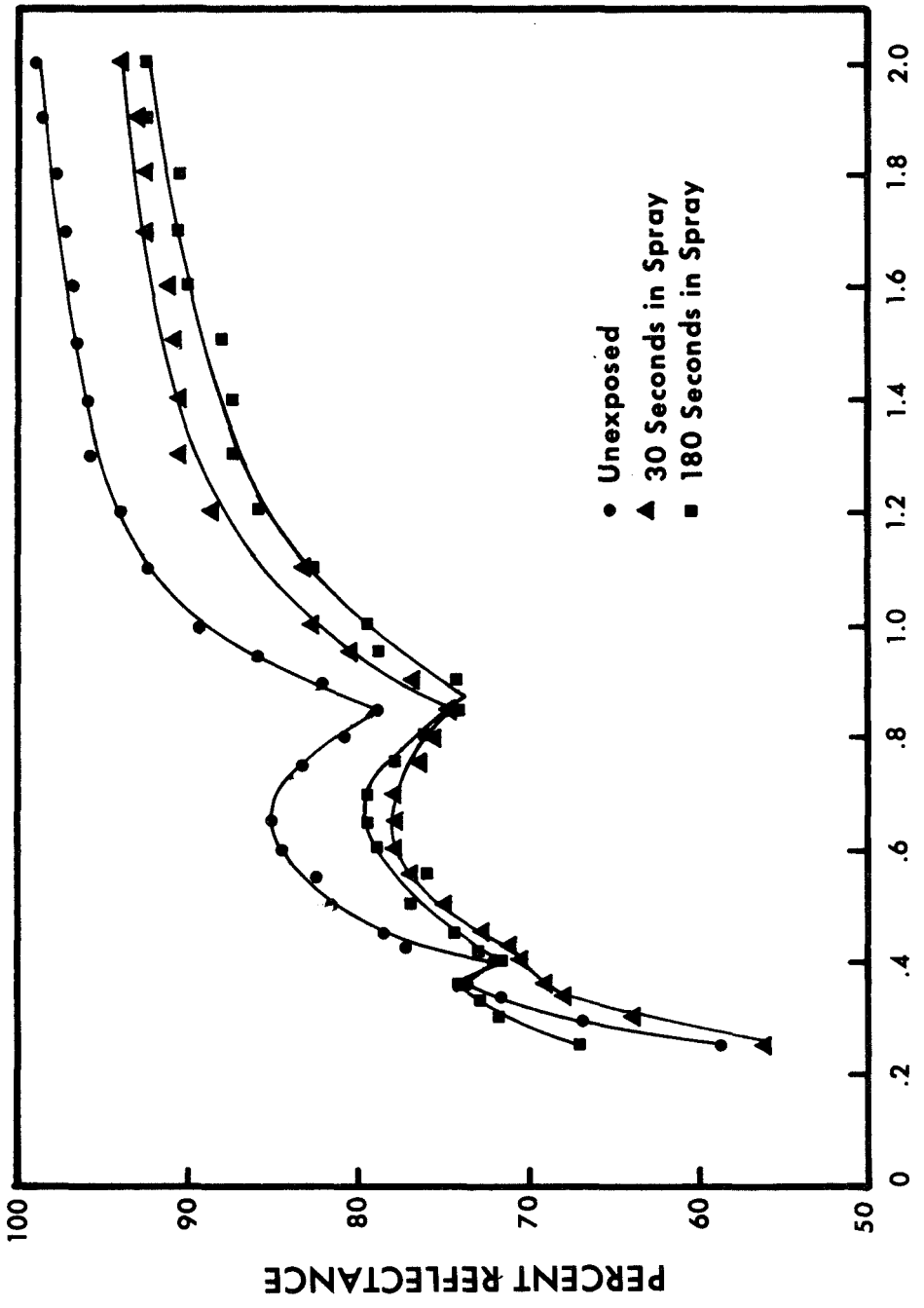

Figure IV-17 Aluminum Foil Reflectance Data (30 and 180 Seconds Exposure)

In the shorter wavelengths the reflectance values fluctuated on either side of the unexposed sample. The reason for the fluctuation is the great dependency of reflectance values on the precise location of the sample with reference to the incoming beam. As opposed to the paint samples, the reflectance values of the foil changed as much as 8% with a slight rotation in the sample location. The high specular reflectivity of aluminum foil is the cause for the wide variation in values. Since the only provision for locating the sample's position within the sphere was visually aligning the marks made on the sample holder, the fluctuation in reflectance values was understandable.

CHAPTER V

CONCLUSIONS AND RECOMMENDATIONS

The objective of this study was to determine the effect of water impinging on a surface under space conditions. The scope of the investigation was narrowed by using a single paint sample (92-007) to study such variables as sample temperature before bombardment, the amount of water vented, injection pressure and temperature of water before injection. It was believed that maximum degradation of the sample would occur under one or a combination of these variables. Degradation of this sample was not influenced by any of the variables.

Three different samples (92-007, S13G and Z93) were selected for testing because of their excellent optical properties. No noticeable surface damage to two of the paints (92-007 and S13G) could be detected visually or by reflectometer measurement. The presence of silicone made the paints very resilient and was the prime reason for their lack of degradation. Upon impact of the spray, the paints acted as a spring mass damper system and showed no permanent deformation. The coatings were compressed, absorbing the particles' momentum as a spring might. As the coatings began to resume their original configurations, the particles were accelerated away from the samples. These paints maintained their desirable thermally-controlled properties after bombardment.

Motion pictures of the spray action confirmed the belief that the water droplets were not frozen completely. The particles splattered on impact, indicating that they consisted of thin shells of ice

surrounding liquid centers. The presence of liquid centers explains the build-up of ice on paint samples during testing.

Another reason for the lack of measureable degradation is believed to be the inefficiency of the measuring device. Although the Z93 paint was visibly damaged, the 8-inch reflectometer was unable to measure a change in reflectance. There are two reasons for the sphere's ineffectiveness. First, the paint was eroded in some areas, but it still covered the entire plate. Second, the angle of incidence was not large enough to detect the indentations on the paint's surface.

Conclusions

Limited conclusions can be made because the water droplets failed to freeze solidly before impingement. While results were significantly restricted because of the inability to obtain a solid freeze of the droplets within the chamber, the investigation does add important data to the analytical work done by Mr. Steddum [8] and Mr. J. A. Simmons [7]. Both Messrs. Steddum and Simmons performed studies to determine the time required to freeze water when vented into a vacuum. Mr. Simmons set an upper limit on the freezing time of 327.5 milliseconds, assuming a finite conductivity within the water droplets. Assuming an infinite conductivity, Mr. Steddum estimated the freezing time for similar spherical droplets to be 34.8 milliseconds. The author's investigation showed that water droplets are not completely frozen after 124 milliseconds in a space environment, thus indicating the freezing time reported by Mr. Simmons are closer to the actual time required.

One important contribution made by this investigation is the certainty of damage to the Z93 painted surfaces when struck by vented water. It is recommended that the reflectance of Z93 be the subject of continued

study using a reflectometer that would permit a greater variability in the angle of incidence. This would more effectively measure the amount of degradation caused by the water spray.

Another area of investigation recommended is the study of thermal stresses induced in aluminum due to the rapid cooling caused by the water spray. As mentioned previously, the sample temperature dropped $65^{o}F$ in less than four seconds. This rapid cooling process could result in serious stress problems. Particularly, would this be true if the temperature of the surface being struck by an unfrozen spray was much higher than the original temperature of the sample tested -- namely, $42^{o}F$.

Recommendations for Reflectometer Improvements

The effectiveness of the reflectometer could be increased by making the following modifications:

1. Machine two hemispheres so that when joined together, they will have a minimum of discontinuity at their junction.
2. Paint the inside of the sphere with a highly reflective, diffuse white paint (Nextel Velvet Coating 101-A10 White); thereby, minimizing the problem of a specular surface if flaking occurs.
3. Replace the side-on photomultiplier with an end-on sensing element.
4. Place both detectors in the same housing positioned below and slightly behind the sample holder. This change will minimize shadowing

by the sample holder, giving greater assurance that both detectors will sense the same amount of energy.

5. Place a highly transparent diffuse glass in the sphere's detector openings. This will help compensate for the angular sensitivity of the detectors.
6. Reduce the area of the entrance opening to decrease light losses. It is suggested that the 1.0 inch circular hole be changed to a 3/16 x 1.0 inch rectangular opening.
7. Attach stops to the sample holder for rotation in and out of the beam's path. This change will make certain that the beam strikes the sample at the same point for each measurement.
8. Modify the sample holder so that larger angles of incidence can be achieved.
9. Use amplifiers to obtain the desired signal response, thus eliminating the need for continuously adjusting the slits of the monochromator.

REFERENCES

1. Beauchene, J. H., and P. R. Dennis, "Simulation of the Sun," Optical Spectra, March 1970, pp. 48-52.

2. Edwards, D. K., J. T. Gier, K. E. Nelson, and R. D. Roddick, "Integrating Sphere for Imperfectly Diffuse Samples," Journal of the Optical Society of America, Vol. 51, 1961,

3. Pinson, J. D., "Synergestic and Accelerated Testing Effects on Space Thermal-Control Materials," Ph.D. Dissertation, Oklahoma State University, 1967.

4. Plunkett, J. D., "NASA Contributions to the Technology of Inorganic Coatings," NASA SP-5014, November, 1964.

5. Newnam, B. E., "Error Analysis of the Integrating Sphere Reflectometer Designed by Edwards, et al." TRW Systems, 67-3346 11w-09, April, 1967.

6. Safwatt, H. H., "Effect of Centrally Located Samples in the Integrating Sphere," Journal of the Optical Society of America, Vol. 60, No. 4, pp. 534-41, April, 1970.

7. Simmons, J. A., R. D. Gift, and M. Markels, "Investigation of Effects of Vacuum on Liquid Hydrogen and Other Cryogens Used on Launch Vehicles," Final Summary Report, Contract Number NAS8-11044, (NASA Assession X65-12159), Atlantic Research Corporation, December, 1964.

8. Steddum, R. E., "Characteristics of Water Sprays Under Vacuum Conditions," Ph.D. Dissertation, Louisiana State University, 1971.

9. Wiebelt, J. A., "Engineering Radiation Heat Transfer," New York: Holt, Rinehart and Winston, 1966.

10. Williams, R. A., "Construction and Analysis of a Long Wavelength Integrating Sphere Reflectometer," Ph.D Dissertation, Oklahoma State University, 1967.